NASA/TM—2006-214241

Fan Performance From Duct Rake Instrumentation on a 1.294 Pressure Ratio, 725 ft/sec Tip Speed Turbofan Simulator Using Vaned Passage Casing Treatment

E. Brian Fite
Glenn Research Center, Cleveland, Ohio

April 2006

NASA STI Program . . . in Profile

Since its founding, NASA has been dedicated to the advancement of aeronautics and space science. The NASA Scientific and Technical Information (STI) program plays a key part in helping NASA maintain this important role.

The NASA STI Program operates under the auspices of the Agency Chief Information Officer. It collects, organizes, provides for archiving, and disseminates NASA's STI. The NASA STI program provides access to the NASA Aeronautics and Space Database and its public interface, the NASA Technical Reports Server, thus providing one of the largest collections of aeronautical and space science STI in the world. Results are published in both non-NASA channels and by NASA in the NASA STI Report Series, which includes the following report types:

- TECHNICAL PUBLICATION. Reports of completed research or a major significant phase of research that present the results of NASA programs and include extensive data or theoretical analysis. Includes compilations of significant scientific and technical data and information deemed to be of continuing reference value. NASA counterpart of peer-reviewed formal professional papers but has less stringent limitations on manuscript length and extent of graphic presentations.

- TECHNICAL MEMORANDUM. Scientific and technical findings that are preliminary or of specialized interest, e.g., quick release reports, working papers, and bibliographies that contain minimal annotation. Does not contain extensive analysis.

- CONTRACTOR REPORT. Scientific and technical findings by NASA-sponsored contractors and grantees.

- CONFERENCE PUBLICATION. Collected papers from scientific and technical conferences, symposia, seminars, or other meetings sponsored or cosponsored by NASA.

- SPECIAL PUBLICATION. Scientific, technical, or historical information from NASA programs, projects, and missions, often concerned with subjects having substantial public interest.

- TECHNICAL TRANSLATION. English-language translations of foreign scientific and technical material pertinent to NASA's mission.

Specialized services also include creating custom thesauri, building customized databases, organizing and publishing research results.

For more information about the NASA STI program, see the following:

- Access the NASA STI program home page at *http://www.sti.nasa.gov*

- E-mail your question via the Internet to *help@sti.nasa.gov*

- Fax your question to the NASA STI Help Desk at 301–621–0134

- Telephone the NASA STI Help Desk at 301–621–0390

- Write to:
  NASA STI Help Desk
  NASA Center for AeroSpace Information
  7121 Standard Drive
  Hanover, MD 21076–1320

Fan Performance From Duct Rake Instrumentation on a 1.294 Pressure Ratio, 725 ft/sec Tip Speed Turbofan Simulator Using Vaned Passage Casing Treatment

E. Brian Fite
Glenn Research Center, Cleveland, Ohio

National Aeronautics and
Space Administration

Glenn Research Center
Cleveland, Ohio 44135

April 2006

Fan Performance From Duct Rake Instrumentation on a 1.294 Pressure Ratio, 725 ft/sec Tip Speed Turbofan Simulator Using Vaned Passage Casing Treatment

E. Brian Fite
National Aeronautics and Space Administration
Glenn Research Center
Cleveland, Ohio 44135

Summary

A method of reducing noise in modern, high bypass, turbofan aircraft engines is to reduce the tip speed of the rotating components, as part of an overall cycle change. During the Advanced Subsonic Technology program, a low tip speed fan was designed by Pratt & Whitney and tested at the NASA Glenn Research Center 9- by 15-Foot Low Speed Wind Tunnel (LSWT) to document fan acoustic and aerodynamic performance. The goal was to demonstrate fan noise reductions that contribute to meeting the overall program goal of 10 dB in aircraft noise reduction relative to a 1992 baseline. The fan aerodynamic design point (cruise, 0° setting angle) tip speed was 725 ft/sec with a total pressure ratio of 1.294, and a corrected weight flow of 42.5 $lb_m/s/ft^2$. The fan design includes variable pitch with spherical tip geometry. The low tip speed design resulted in concerns with regard to sufficient operating range, especially when operating in the presence of inflow distortion. To address this concern, a casing treatment was designed that used recirculation to extend the fan stall line and provide an acceptable operating range. The casing treatment is a full annular treatment that extracts air downstream of the fan mid-chord, straightens it, and injects it back into the flow stream upstream of the fan mid-chord. Variations of the treatment were tested to evaluate moving the air extraction and insertion axial locations and evaluating the impact on performance, operability, and noise. First, the overall aerodynamic experimental results are presented for this low tip speed, low noise fan without casing treatment. An unusual instability was discovered just beyond the design operating line (toward stall) which required modified test procedures to allow the fan performance to be mapped along an entire speed line. Next, overall aerodynamic experimental results are presented for the fan using several variants of the casing treatment. Measurements were made to compare stall margin improvements as well as measure the performance impact of the casing treatments. Then, the experimental results in the presence of simulated inlet distortion, via screens, are presented for the baseline and recirculation casing treatment configurations to again determine the impact on stall margin. Finally, estimates are made for the quantity of recirculation weight flow based on limited instrumentation in the recirculation system along with discussion of results and conclusions.

Introduction

The National Aeronautics and Space Administration is working to advance the understanding of technology that will enable reductions in acoustic emissions of aircraft engines. As part of the Advanced Subsonic Technology program, milestones for aircraft noise reduction called for a reduction of 10 dB at each of the three aircraft measurement locations; approach, sideline, and takeoff, relative to a 1992 baseline (ref. 1). This translated into an engine noise reduction of 6 dB at each of these measurement locations. To meet these goals, various technologies are being studied for engines as well as the entire airframe. One proposed concept for engine noise reduction is an overall cycle change that accommodates reduced tip speeds for the fan. A reduction in fan tip speed results in lower noise as described in reference 2. To study possible designs that meet this goal, Pratt & Whitney designed fan stages with reduced tip speed for aerodynamic and acoustic assessment in the NASA Glenn 9- by15-Foot LSWT. The

first of the AST supported fans was called Fan 1 and the design details are described in Hobbs, et al. (ref. 3). Experimental assessment of Fan 1 showed improved noise emissions with good aerodynamic performance. The aerodynamic performance is described by Jeracki (ref. 4) and the acoustic performance by Dittmar, et al (ref. 5). The design point for this fan was a pressure ratio of 1.294 at a tip speed of 806 fps. Conclusions drawn from testing this fan showed a reduction in noise consistent with the tip speed reduction per scaling laws described in reference 2. Based on these results, a second fan, called Fan 2, was designed with still lower tip speed to pursue this noise reduction idea further. Fan 2 represented a 10 percent reduction in tip speed relative to Fan 1 while attempting to maintain identical performance with respect to pressure rise and mass flow. This results in increased fan loading to achieve the desired fan design performance parameters. Table 1 summarizes the fan design parameters for Fans 1 and 2. The detailed design of Fan 2 is described by Neubert, et al. (ref. 6) and the detailed experimental acoustic results are described by Elliot, et al. (ref. 7). One purpose of this paper is to document the overall experimental aerodynamic performance of Fan 2 in support of the acoustic testing. Another purpose is to document the experimental aerodynamic performance of several casing treatment designs tested with Fan 2.

A novel technology included for experimental evaluation was a casing treatment that recirculated flow that was extracted downstream of the fan mid-chord and re-injected upstream of the fan mid-chord to improve stall margin. The operating philosophy for these devices is described by Koff, et al. (ref. 8) but the performance sensitivity to axial changes in extraction/injection locations was unknown. The design intent was to extract low momentum flow at the outside diameter flow path wall, pass it through a set of vanes to remove the swirl velocity component, and inject the flow upstream through a slot with improved momentum characteristics. Several configurations of this device were tested with varied extraction and injection axial locations, as well as some flow variation. Hathaway (ref. 9) presents a similar analytical investigation which surveys, using CFD, the affect of altering injection and extraction locations. This work illustrates the detailed flow physics believed responsible for the operability and performance changes. In the current work, these devices showed various levels of effectiveness at extending the stall point, especially in the presence of inlet distortion. Additionally, any device that alters the flow upstream or in the vicinity of the fan tip may change the acoustic performance. These devices pose an acoustic concern since upstream flow disturbances that create fan inflow distortions have shown increases in fan noise in past experiments. The intent of this experiment was to fully evaluate the concepts in terms of aerodynamic, operability, and acoustic performance. Variations on this concept have been tested and shown to generate favorable aerodynamic performance benefits. Suder, et al. (ref. 10) and Stasizar, et al. (ref. 11) have reported stall management benefits from end-wall recirculation using circumferentially discrete extraction and injection locations for a compressor stage. Their assertion is that discrete injection requires less mass flow to gain substantially similar improvements in stall performance enhancement. No acoustic assessment was made for these test configurations. A fan presents a more noise-sensitive implementation than a compressor, at least for current engine noise source composition, and therefore acoustic measurements were made for several configurations to assess acoustic sensitivity to the injection/extraction scheme for this work. Corresponding acoustic data evaluations are presented by Elliott (ref. 7), however, some summary plots in this paper will include the overall acoustic performance for relative comparisons.

Nomenclature

A	area
EPNdB	Effective Perceived Noise, dB
P	pressure, psi
π, PR	pressure ratio, $\dfrac{P_{t2}}{P_{t1}}$ ratio of total pressure downstream of fan to free stream total pressure
rpm	fan model rotational speed in revolutions per minute

SM	stall margin, percent, $\dfrac{WF_{opline}}{WF_{stall}} \times \dfrac{\pi_{stall}}{\pi_{opline}} \times 100$

T temperature, degrees Rankine

TR temperature ratio, $\dfrac{T_{t2}}{T_{t1}}$ ratio of total temperature downstream of fan to free stream total

                          temperature

V Velocity

WF weight flow, lb/sec

ρ density

ϕ stalling flow coefficient, $\dfrac{WF}{\rho A U_T}$

$\Delta\phi$ change in stalling coefficient

Subscripts

b Baseline condition
c Corrected to standard day conditions
t Total pressure or temperature
T Tangential component
1   Upstream conditions
2   Downstream conditions
$stall$ Quantity at condition corresponding to fan stall point
$opline$ Quantity at condition on the design operating line

Apparatus and Procedure

Fan Package

    The fan system consists of a variable pitch fan and rotor assembly with 18 composite fan blades, a set of 51 guide vanes with moderate radial bow at the tip, and a flight-like nacelle. The pitch of the fan was set manually by installing interchangeable blade base locking devices in the hub. The tip cut is spherical to provide a uniform tip clearance at all setting angles and the fan root to hub clearance allows for a change in angle from cruise to reverse thrust. The cruise setting angle was arbitrarily chosen as zero, takeoff was –8° (more open), and reverse thrust required a change to plus 110°. Figure 1 shows a cross section of the model and figure 2 is a photo of the model installed in the 9- by 15-Foot LSWT. The core was simulated in a passive manner meaning that flow through the core was driven by pressure differential—no core turbomachinery was included in the model. The nacelle pictured in figure 2 is the "flight" nacelle configuration used for acoustic testing. The performance testing configuration replaces the inlet with a bellmouth and the nozzle with a variable fan exit nozzle (VFEN). This configuration is used for fan mapping and is shown in figure 3. Several rub strips were used during different test segments. A smooth rubstrip was used during all baseline acoustic testing. A rubstrip with penetrations for laser tip deflection measurements was used for baseline aerodynamic performance testing. As previously discussed, several configurations of rubstrips that included an advanced casing treatment, called Vaned Passage Casing Treatment (VPCT) (ref. 8), were also tested to determine effects on stall margin and acoustic performance with the low tip speed fan for clean and distorted inflow. All of the rub strips included abradable material over the fan tip region that is identical to material used in some commercial aircraft engines.

Test Facility

The test was conducted in the NASA Glenn 9- by 15-Foot LSWT. This test section can achieve Mach numbers to 0.23 and is anechoic to 400 Hz to permit acoustic testing of concepts using tunnel flow. Performance tests, using the bellmouth and VFEN configuration, were run at Mach 0.04 for flow clean-up into the inlet, thereby ensuring uniform flow into the fan. A complete description of the facility and capabilities is available in reference 12.

Free stream inlet conditions were measured upstream of the model using either a cruciform rake as shown in figure 4 during performance testing or with one of two facility rakes, one at the inlet to the test section and the other adjacent to the model, mounted on the test section ceiling during acoustic testing. The cruciform rake, when installed, was mounted on the model centerline approximately 36 in. upstream of the bell mouth highlight. The facility ESCORT data system was used for acquiring and storing all steady-state total pressure, total temperature, and static pressure data as well as values for balance forces and tip clearance. Measurement accuracy for pressures is 0.008 psi and for temperature 0.73 °F. These accuracies in measured quantities lead to an uncertainty for calculated pressure ratio of 0.6 percent, temperature ratio of 0.2 percent, and efficiency of 2.9 percent. The bellmouth mass flow measurement is accurate to 0.5 percent.

Model

All data included in this report were acquired using the model in the performance configuration shown in cross section in figure 5. The model axial station reference location was the rotor pitch change axis and was defined as station 170.0 in. The angular reference used was 0° located at TDC and positive angle measured counter-clockwise when the rotor was viewed from upstream looking downstream. A bellmouth inlet, calibrated using CFD, was used to measure weight flow using eight static pressures measured at the weight flow station shown in figure 5. The bellmouth can also accept inlet rakes at Station (STA) 2.0 for measuring inlet distortion. Penetrations are provided to accommodate a total of eight rakes. This test had available four total pressure pole, or inflow, rakes (eleven Pt probes each) and four total pressure boundary layer rakes (nine Pt probes each). Figure 6 shows the inlet rake array installed in the flight inlet, however, the bellmouth array was identical. These rakes allow for measurement and correction, if desired, for the fan inlet total pressure reductions caused by the boundary layer, distortion screens, angle of attack, etc. For the data later described, these rakes were used to measure the inlet conditions for the inlet with a distortion screen installed. A ring of static pressures was installed at the same model station as the STA 2.0 rakes.

Combination rakes at STA 12.5 were used to measure the fan pressure and temperature rise. These rakes incorporated a total pressure and a total temperature probe at each of 10 radial stations along the rake as shown in figures 5 and 7. These rakes provided the data for the radial profiles of bypass total pressure, total temperature, and efficiency presented in the experimental results. A ring of static pressures was located co-planar with the STA 12.5 probe axial location on both the outer diameter and inner diameter of the bypass duct. A linear curve fit was used to interpolate these duct static pressures which was used along with the corresponding measured total pressure value to calculate the local Mach number at each STA 12.5 probe radial location, which was later used to calculate data corrections. The total temperatures measured with the rakes at STA 12.5 had applied both recovery (using the calculated local Mach number) and wire corrections to adjust the measured quantities. Details of these corrections are described in reference 4. To measure flow conditions entering the simulated core, two arrays of five total pressure and two arrays of five total temperature probes were mounted along the span of the core inlet guide vanes as shown in figures 5 and 7. Likewise these also had corresponding static pressure taps on the core inner diameter and outer diameter at the probe axial station, four on the inside diameter and four on the outside diameter. The core also included two combination rakes at the core weight flow station shown in figure 5. Each of these included five total pressure and five total temperature probes to cover the core flow duct span. Again, four static pressure taps were placed on the inner and outer diameter of the core flowpath at the weight flow rake axial station for calculating recovery coefficients. Again the core total

temperature measurements included corrections for recovery performance and wire effects as described in reference 4. Bypass weight flow was calculated by subtracting the weight flow measured by the core weight flow rakes from the bellmouth total flow measurement.

During fan mapping, strain gages were installed on six fan blades to monitor stresses for safe operation, warn of unexpected instabilities, and detect stall. Gages were mounted to detect primary fan blade structural modes and were used throughout performance testing. Consistent strain limits were used throughout the test and an automatic shutdown system was employed. These procedures serve to make stall point detection relatively consistent for each configuration tested. Additionally, during initial performance testing, fan blade tip clearance was measured using a proprietary Pratt & Whitney optical tip clearance system with eight sensors to monitor leading and trailing edge tip clearance at four locations around the fan case circumference, 45°, 135°, 225°, and 315°. The design intent was to have the fan clearance be between 0.050 and 0.055 in. at takeoff (7850 rpmc). This clearance was selected as the "end of life" clearance and was thought to be the worst case for fan performance in terms of stall margin, operability, and performance.

Casing Treatment Description

In addition to the low tip speed fan, one of the key technologies to be evaluated was an advanced casing treatment, VPCT, being developed by Pratt & Whitney (ref. 8). The fan design utilized the casing treatment to assure adequate stall margin using a low tip speed fan. To investigate aerodynamic and acoustic performance sensitivity, several configurations of the VPCT were evaluated. The modular design of the VPCT model hardware allowed for interchangeable segments to alter the VPCT configuration. The parameters varied were the axial position of the flow extraction and injection slots in the vicinity of the fan tip and the amount of recirculation flow utilized. The VPCT configurations tested for performance are shown in figure 8. The VPCT tested and reported in reference 4, is shown for reference at the top left and is the Fan 1 VPCT configuration. The remaining assemblies labeled VPCT 1 through VPCT 8 were designed and built for Fan 2. The baseline casing treatment, VPCT 1, had the flow extraction and the flow injection axially located within the blade passage. VPCT 2 moved the injection point upstream of the rotor leading edge as shown in figure 8. VPCT 3 moved the extraction location downstream of the trailing edge while the injection point remained over the rotor. VPCT 4 moved the extraction location aft of the blade trailing edge, same as VPCT 3, but increased the flow through the VPCT. VPCT 5 moved the injection location forward and the extraction point aft, both locations moving out of the blade passage but using the baseline injection flow while VPCT 6 used this configuration with increased recirculation flow. VPCT 7 was the base configuration with reduced injection flow. Finally, VPCT 8 was the baseline configuration with the flow shut off to evaluate the cruise penalty for a VPCT with the recirculation flow turned off. Table 2 summarizes the casing treatment configurations tested during the entry, however, the amount of data available for each configuration varied depending on the test interest and test time available.

Experimental Results and Discussion

Design Point

Although nearly all of the data was acquired and will be presented for the off-design operating conditions of takeoff, cutback, and approach, limited data was acquired at the design condition, or cruise, to compare measured fan performance with the design goals. The cruise condition used a blade stagger angle of 0° (by definition, recall setting angle is measured relative to the cruise angle with the takeoff setting angle of −8° used for off-design operation). Fan performance along a speed line was measured at the design rotational speed of 7560 rpmc. This data is shown in figure 9 along with the design intent. The measured fan overall pressure ratio was 1.294 at 91.65 lb/sec corrected weight flow: the design intent was 1.294 at 91.96 lb/sec corrected weight flow. The weight flow difference from design intent is

0.34 percent (which is actually within the measurement capability of approximately 0.5 percent). Visible along the speed line at just above 90 lb/sec flow rate (see note on fig. 9) is a region where the fan operating point changed, in a detrimental way and rather abruptly, to a condition of lower pressure ratio and efficiency (as will be shown later). This change was unexpected and is labeled as "instability" since the fan wanted to operate only at stable points at the boundaries of the transition region. Normally a complete map would be generated including several rotational speeds with continuous speed lines generated by back pressuring the fan using the variable fan exit nozzle. A notable characteristic of this fan is that the speed lines are discontinuous at the higher rotational speeds just beyond the operating line. The unusual instability encountered resulted in high fan blade stresses and prevented a continuous speed line test procedure. The eventual test procedures to obtain a speed line were as follows: speed lines were generated on the choke side of the instability, the VFEN area was opened and model rotational speed reduced, the VFEN was closed to transgress the instability region, the model speed was then increased to the desired speed(s) and the remaining data of interest was acquired. An ESCORT data feature called "continuous cyclic" was used to acquire data adjacent to high stress conditions. This allows automatic 1.0 second data scans for all steady state values while a region of potential high fan blade stress is investigated. The scans are reviewed during post processing and only the last data point deemed "good" is processed and utilized in subsequent calculations.

The design point radial profiles for pressure and temperature ratio, along with efficiency are shown in figure 10. The gap in the span wise data reflects the presence of the flow path splitter between the bypass and core ducts. The smooth case was used for these measurements meaning no VPCT was applied. The pressure profile indicates a drop near the tip as was intended by design. The temperature ratio increases significantly outboard of the 10.685 in. radial measurement resulting in a significant drop in efficiency from 84.9 to 71.9 percent at the largest radial measurement location of 11.119 in. The five inboard radial locations show measurements at the core inlet location and, as expected, the fan performance is lower at the inboard locations. The overall predicted fan adiabatic efficiency was 95.1 percent, compared with a measured value of 91.6 percent. This value is 3.6 percent lower than predicted but the measurement accuracy was probably affected by the limited radial measurement locations and the difficulty in measuring the efficiency of a fan with such a low temperature increase. Data acquired during this entry and data reported in reference 4 indicate the efficiency data repeats within 0.1 percent, however, the accuracy is ±2.9 percent as previously stated.

Baseline—Clean Inlet

The primary purpose of this test was to measure the acoustic performance of the low tip speed fan and the casing treatments. Therefore, most data acquired was for the blade stagger angle of –8°, or takeoff, with limited data acquired at the cruise setting angle of 0°. The data presented are for the –8° stagger with the model in the performance configuration using various casing treatment configurations as previously described. The casing treatment is generally considered of most benefit at takeoff and landing where the possibility of inlet distortion is most probable making these configurations of most interest. Unless otherwise noted, all values for weight flow and rotational speeds are corrected to standard day conditions. In addition, the bypass and core data from individual rakes are combined using an area average for the bypass rakes and core rakes separately providing an area average core and bypass value. Then these area average values are combined using a mass average for the core and bypass to get overall values for pressure rise and efficiency for the fan. The high bypass ratio (11+) means the bypass data are weighted much more than the core data reducing the impact of the core on the overall performance. Nonetheless, the data in the core show significantly reduced performance and do impact, slightly, overall fan performance parameters. Additionally, it is likely that since a passive core is used in the model, the as-tested values do not directly correlate to what may be expected with a powered core. The core mass flow was set using the core exit nozzle area which was specified during the model design using CFD analysis to get the appropriate bypass ratio.

The fan total pressure map for the baseline configuration is shown in figure 11. Speed lines are plotted for several corrected rotational speeds including 4420 (approach), 6950 (cutback), and 7875 (takeoff). Again, a significant drop in fan performance across the region of instability is observed. In fact, the magnitude of the change in pressure ratio across the instability region is much larger when compared to the design point data and the overall region bounded by the instability is larger as well. A drop in pressure rise as well as efficiency (to be quantified later) was observed. This was an interesting, though problematic and unwelcome phenomenon discovered in the fan operating range.

The speed line for the approach condition shows a dramatic change in weight flow between data points at 49.4 and 53.6 lb/sec. This is caused by the model operation and is a result of the core starting to pass flow. Recall that the core has no turbo machinery to pump the flow through the core duct. Therefore, the pressure rise required to overcome duct losses must be reached before the core will start. This behavior associated with the core flow starting is only present in data for approach model speeds at very open VFEN settings (large fan bypass exit area).

At the takeoff rotational speed when operating on the design operating line, the baseline fan had a rotor adiabatic efficiency of 94.1 percent and a takeoff stall margin of 22.9 percent. The stall margin is calculated by:

$$SM \equiv 100 \times \left[\left(\frac{\pi_{stall}}{\pi_{opline}} \right) \times \left(\frac{WFc_{opline}}{WFc_{stall}} \right) - 1 \right]$$

The reference condition ("opline" condition in the above equation) is the approximate location where the fan operation crosses the desired cycle operating line for the fan on each speed line. This point would be set by the nacelle exit area for an engine but since the VFEN is being used, setting the exact area to get the operating line condition is difficult. An interpolation was used on the acquired data to get the operating parameters at the approximate operating line intersection. This process, if needed, was used for all of the data reported for this and subsequent configurations.

The baseline fan 2 adiabatic efficiency map for the takeoff stagger angle is shown in figure 12 and shows the trends for several speeds of interest. Smoothed lines are placed through the data points for visualization of each speed line. The data follow expected characteristics until the instability is encountered. The break in each line corresponds to the region on the operating map where the instability prevented fan operation. The efficiency drops significantly across the instability region and the curve flattens as well holding the lower efficiency levels over a wide range in weight flow. For the takeoff condition (7875 rpmc) the efficiency at the instability boundary is 93.4 percent and drops to 91.8 percent for the first point on the stall side of the instability. The efficiency data for the approach condition has a distinct character due to the core start phenomenon discussed previously. The core starts at the 49.4 lb/sec, 90.5 percent efficiency point and the fan operating condition jumps to the 53.6 lb/sec, 94.1 percent efficiency point. Near the middle region of the approach data, there is an efficiency step in the downward direction from 94.4 to 93.1 percent with measured weight flows of 46.79 and 46.89 lb/sec, respectively. Close inspection of the map data in figure 11 reveals these points lay nearly on top of one another but the weight flow actually increases slightly at this point on the speed line. One possible explanation is that the same instability that caused high stresses for other speeds is present here and causing the efficiency and weight flow shifts, yet not strong enough to cause a fan blade stress problem and alter fan mapping progression.

Radial profiles for the fan bypass and core total pressure ratio, temperature ratio and resulting efficiency are shown in figures 13 through 15 for approach, cutback, and takeoff rotational speeds, respectively, on the fan operating line. The total pressure ratio profiles indicate increasing loading as a function of radial span with a reduction in loading occurring from approximately 90 percent span outboard. This is consistent with the fan design intent and is likely enhanced by the large tip gap selected for this test. As previously described, the tip gap selected was an end-of-life gap of 0.050 to

0.055 in. Figure 16 shows that the measured clearance varied around the circumference from a minimum of 0.035 in. at the 45° trailing edge measurement location to a maximum of 0.053 in. at the 315° leading edge measurement location. The clearance at the leading edge was generally larger than the trailing edge and is evident in the data plotted in figure 16. Since the same fan rotor and nacelle build-up was used for all of the casing treatments, the operating tip gap is assumed to be consistent for all of the data; however, it was not measured for the remaining configurations tested. Static checks were used for each hardware configuration to check for a consistent tip gap.

The temperature ratio profile (fig. 14) displays a marked increase in temperature occurring outboard of the 10.685 in. radial measurement, just outboard of radial location where the pressure rise tends to drop off. These observations in pressure and temperature rise are displayed prominently in the adiabatic efficiency profile with a drop from 96.6 to 77.7 percent at the 10.233 and 11.119 in. locations, respectively, at the takeoff speed. These efficiency trends indicate that a tip flow disturbance is likely to have a notable effect on the fan efficiency and performance as a result of the tip biased fan loading profile. Several efficiencies for the approach condition, and also some for the cutback condition, have calculated efficiency greater than 100 percent which is believed a result of the data system accuracy and difficulty in measuring, accurately, the low temperature rise for this fan at these operating conditions. For these reasons, efficiency data is generally presented as a delta from the baseline test configuration.

VPCT–1—Clean Inlet

In general, the total pressure fan map with VPCT–1, shown in figure 17, looks substantially similar to the baseline fan map (fig. 11). The instability just beyond the operating line remained along with the core-start discontinuity at approach speed. As before, all of the speed lines were shifted down and to the left indicating a loss in performance. Other significant differences were also noted. First, the 5800 rpmc speed line could be traversed continuously without stopping to navigate the instability. There remains a drop in performance along this speed line corresponding to the location of the instability but the severity of the instability as monitored through the strain gages was not enough to prevent traversing a continuous speed line to acquire data. Finally, as one would expect, the stall point for each speed line is extended to significantly lower mass flows using the casing treatment. For direct comparison and to better show the stall point extension and the performance loss, figure 18 includes the measured takeoff speed line for both the VPCT–1 and baseline smooth case test configurations. The performance penalty using VPCT–1 is considerable on the choke side of the instability (to the right of the operating line) but is not as large on the stall side (to the left of the operating line and instability region). This may suggest an interaction between the recirculation flow from the casing treatment and the source of the instability, using VPCT–1, which triggers a large reduction in pressure rise and mass flow similar to the instability. The stall margin for VPCT–1 is 27.7 percent at takeoff compared to 22.7 percent for the baseline (smooth case), a 5.0 percent improvement. In terms of mass flow coefficient as reported in references 10 and 11, VPCT–1 provides a 4.6 percent improvement. From Suder et al. (ref. 10), the stalling flow coefficient is defined as

$$\Delta\phi \equiv \left(\left(\phi_{stall}\right)_b - \left(\phi_{stall}\right)\right) \div \left(\phi_{stall}\right)_b$$

Radial profiles for pressure ratio, temperature ratio, and efficiency for the VPCT–1 configuration are presented in figure 19(a) through (c), respectively. The values for both the bypass duct and core duct are shown. A significant drop in pressure rise is apparent in the radial profile data for VPCT–1, especially at the takeoff condition. This is consistent with the map overall pressure ratio drop shown previously. The effect is largest near the tip but extends well inboard to beyond 50 percent immersion for the fan blade. The core values appear essentially unaffected by the casing treatment as one may expect. The impact on temperature ratio is also measurable and shown in figure 19(b) with a significant increase in temperature ratio at the tip resulting in a large efficiency penalty displayed in figure 19(c). The efficiency penalty moderates inboard since, as the pressure rise drops off, the temperature rise also reduces in the mid-span

region of the fan blade resulting in a smaller efficiency penalty. The increase in temperature ratio is not unexpected since some of the tip flow is likely to be recirculated through the blade tip passage several times before it exits the tip region via mixing with the inboard flow. Again, the temperature ratio and efficiency for the core are relatively unchanged between the baseline and VPCT–1 casing treatments. For this reason, subsequent plots of pressure, temperature, and efficiency profiles will not include the values of core data on the plots since the changes are very small and appear insignificant.

Remaining VPCT Configurations—Clean Inlet

Fan total pressure map data presented for the remaining configurations is limited to the takeoff speed line and is shown in figures 20 through 25 for VPCT–2 through VPCT–5, VPCT–7 and VPCT–8, respectively. Each of these plots include the takeoff speed line for each VPCT plotted with the baseline speed line also at takeoff speed (7875 rpmc) for comparison. In each plot, the open symbols are the smooth baseline case or reference data, while the solid symbols are the data for the casing treatment of interest. Also included on each plot is the design operating line and predicted stall line. As with VPCT–1, for each of these VPCT's tested, the takeoff speed line data indicate the pressure rise and weight flow are reduced when the casing treatment is installed, especially on the choke side of the instability boundary. Also notable is the difference in the speed line shift on either side of the instability boundaries. As with the VPCT–1 configuration, on the stall side of the instability, the casing treatment performance is comparable to the smooth case data. This trend seems to suggest the casing treatment may be interacting with the source of the instability and triggering the fan to perform at the lower operating conditions when on the choke side of the instability region. If this is the case, an interesting question is whether the performance debit of the VPCT would be as severe if the instability was not present in the design. The last casing treatment plot is for VPCT–8 which is the "off" configuration with a simple passage block employed to prevent circulation through the treatment. Even with the recirculation flow off, the pressure rise and weight flow show reductions relative to the baseline, although to a lesser degree.

A comparison of radial total pressure profiles, bypass data only, is shown in figure 26(a) and (b) for all of the VPCT's tested and shows that all have a measurable pressure rise deficit when compared to the baseline smooth case configuration. Figure 26(a) shows the overall trends while figure 26(b) is rescaled to allow easier comparison of the data at the outermost radii. The VPCT cases using an aft extraction location are the worst performers in terms of pressure ratio loss while those with a forward injection location are slightly better. The VPCT–8 configuration with the recirculation passage blocked is the closest in performance to the baseline but it too shows a penalty in pressure rise. The radial total temperature profiles for the bypass are shown in figure 27(a) and (b) with (a) being the overall trend and (b) rescaled to show data trends at the outermost radii. As expected the baseline smooth and off (VPCT–8) configurations are the best performers. As with the pressure profiles, the casing treatments with a forward injection location perform slightly better than the configurations with an aft extraction location in terms of temperature rise with lower being better.

The bypass radial adiabatic efficiency profiles calculated using the total pressure and total temperature profiles are shown in figure 28(a) and (b) with the latter plot rescaled to better show data trends at the outer-most radii. The efficiency combines the effects of temperature and pressure performance and continues the observed trends of the pressure and temperature profiles. Again looking primarily at the outermost performance, the baseline has the highest efficiency followed by the off (VPCT–8) configuration, the forward injection configurations, VPCT–2 and –5 are next flowed by the aft extraction configurations (VPCT–5, –3, and –4). The case with both slots in the passage, VPCT–1, falls among the aft cases.

Baseline—Simulated Distortion

In addition to the clean inlet configurations, each configuration was also tested using a simulated inlet distortion designed to measure the performance of each VPCT configuration operating in the presence of

distorted inlet flow conditions. The distortion was generated using a screen designed by Pratt & Whitney and is shown installed in the bellmouth inlet in figure 29. The screen was located at model station 160.0, 10 in. upstream of the fan stacking axis, was centered at bottom dead center, and covers an arc of 145° in the inlet. The distortion produced is measured at STA 164.44 in. (also called STA 2.0) through a set of static pressure measurements at the wall along with pole and boundary layer rakes installed to measure total pressure downstream of the distortion screen. The rake layout is shown in figure 6 for the flight inlet but the bellmouth rake configuration is identical. The distortion measured by the pole rakes is shown in figure 30 and by the boundary layer rakes in figure 31. Both figures include data outside the influence of the distortion screen for reference. The overall distortion parameter was 19 and 21 percent for the pole rakes and boundary layer rakes, respectively. The distortion parameter is the difference between the maximum and minimum total pressure divided by the free stream total pressure for each set of rakes.

The take off fan total pressure map for the baseline configuration with distortion is shown in figure 32 with the smooth wall casing takeoff speed line plotted for reference. It is obvious the distortion has a pronounced effect on the operating range of the fan as measured in the clean configuration. The stall margin for this case, based on measurements, is 5.2 percent or a drop of 17.7 percent relative to the clean inlet stall margin. The fan pressure rise and weight flow are also reduced significantly as shown by the speed line shifting down and to the left when distortion is present. The speed line data was acquired in a continuous manner as blade stresses were not above limits, however, significant strain gage activity was present due to the distortion and possibly due to some additive component produced by the instability as well.

VPCT–1—Simulated Distortion

The take off total pressure map for VPCT–1 with inlet distortion is presented in figure 33. The take off speed line for the baseline clean and distorted inlet cases is also plotted for comparison. The most significant observation is the remarkable improvement in stall margin relative to the smooth wall when distortion is present. VPCT–1 provides a stall margin of 24.0 percent, an 18.8 percent improvement in stall margin over a smooth case. In fact, the smooth and distorted stall margin using VPCT–1 only varies by 3.7 percent as compared to a drop of 17.5 percent for the baseline smooth test case.

Remaining VPCT Configurations—Simulated Distortion

The take off total pressure map of the remaining VPCT configurations tested with distortion is shown in figures 34 through 37 which includes VPCT–2 (fwd inj), –3 (aft extr), –5 (fwd inj & aft extr), and –7 (–1 reduced flow). The stall margin improvement for VPCT–1 and VPCT–2 are very similar with VPCT–2 generating a stall margin of 23.3 percent or an improvement of 18.1 percent over the baseline smooth configuration. The remaining configurations showed less, but still significant, improvement in stall margin relative to VPCT–1 and VPCT–2. The stall margin for VPCT–3 and VPCT–4 using aft extraction locations is 20.0 and 19.3 percent, respectively. Arguably, this data would suggest that an aft extraction location for the recirculation flow is somewhat less effective than a passage location. This is likely due in part to greater total pressure loss as the flow extraction is delayed, causing more blockage downstream. Some contribution could also be from added capacitance or lag in the recirculation system decreasing the effectiveness for an extraction location moved further downstream. The last configuration tested with distortion, VPCT–7, which is a reduced flow version of VPCT–1 showed the least stall margin improvement with a stall margin of 18.5 percent, still a 13.3 percent improvement over the smooth wall baseline. VPCT–7 would be expected to have less operability improvement than VPCT–1 by reducing the recirculation flow through the casing treatment by reducing the area at the injection exit of the VPCT.

Casing Treatment Recirculation Flow

Finally, the VPCT performance is dependent on the mass flow through the recirculation duct of each casing treatment configuration as well as the location of extraction and injection locations (ref. 9). The casing treatments tested were designed to be as "flight-like" as possible and while making the test very realistic in terms of installation and installed operability impact, some parameters, such as the weight flow, were difficult to measure. Unlike work presented in references 10 and 11, the hardware and test plans did not include use of an external supply and extraction which would allow use of accurate flow meters to measure injected and extracted flow. For the VPCT configurations tested, internal instrumentation is used to make estimates of the weight flow passing through the recirculation passage for each VPCT. The instrumentation layout is shown in figure 38 and includes static pressures, total pressures, and total temperatures. The recirculation duct entrance, before the internal turning vanes, includes total and static pressure instrumentation at two circumferential locations while the exit instrumentation downstream of the internal turning vanes includes total temperature in addition to static and total pressure. The total temperature measured at the exit of the VPCT was also used as the inlet total temperature. The exit calculation of weight flow is rather straight forward using the Ps and Pt to get a Mach number, calculate a static temperature, calculate the static density, use the temperature to get the speed of sound, with this a velocity is determined and weight flow (unadjusted) is calculated from:

$$WF = \rho \times A \times V$$

Unadjusted refers to lack of any correction for blockage effects since the measurements are on, or near, the centerline of the recirculation passage. For blockage adjustments, values extracted from numerical calculations, performed by Pratt & Whitney, were used to adjust the inlet and exit centerline values to account for blockage effects. An additional correction was applied to the flow at the inlet (or extraction location in the casing) of the VPCT. The flow extracted at the casing wall includes swirl from the fan as it has not passed through the stator inside the VPCT (or in the fan stage for that matter). The instrumentation measures the total properties with swirl so the inlet values were also corrected for the swirl in the tip flow. The tip swirl angle, modified to account for the change in radius to the VPCT passage measurement location, was used to adjust the inlet flow for swirl and get the axial components to calculate mass flow. Finally, for comparison, all weight flows were also corrected to standard day using the inlet conditions. Since limited data is available to calculate the mass flow, and at only two circumferential locations, the accuracy of the weight flows is unknown and it is likely that significant differences could exist between the calculated flows and the true flows through the VPCT recirculation duct. Since the same instrumentation is used for all VPCT configurations, it is expected the relative comparisons between configurations make trends observable in the weight flow data but comparisons to other stall enhancement flow recirculation concepts could be misleading.

The VPCT performance in terms of weight flow and stall margin is shown in figure 39. First, it is apparent that even though VPCT–8 was supposed to be off meaning no flow, there remained some limited flow as indicated by the available instrumentation. This supports the radial total pressure profile for this configuration in figure 26, discussed previously, which showed relief at the fan tip through a reduction in total pressure as compared to the baseline smooth fan case. Since the recirculation passage was shut-off by a blocking tang with a metal-to-metal interface, it is possible some flow remained. This would tend to indicate that a threshold flow exists below which, the stall margin will actually be decreased. VPCT–7 is a reduced flow version of VPCT–1, and indeed, it does flow less as designed. VPCT–3 is flowing more than VPCT–1 although the duct geometry is identical with the extraction location moved downstream for VPCT–3. This is not unexpected as the overall pressure rise is likely to be higher downstream of the blade passage and is reflected in the measured mass flows. In general, the casing treatment mass flows are clustered between 2 and 3 percent of fan flow and provide 3 to 5 percent of stall margin improvement over the baseline smooth case configuration. For comparison, figure 40 shows the change in stalling flow coefficient versus percent of fan flow. The same trends are present in this plot and, in general, a 2 to 3

percent recirculation flow provides a stalling flow coefficient improvement of between 3 and 5 percent depending on the VPCT configuration selected.

References 10 and 11 utilize noncontiguous blowing areas in the circumferential direction and suggest that the circumferential mass average injection velocity is a better parameter for indicating stall margin improvements. Discrete injection serves to possibly simplify the system integration and could use less flow depending on the overall effectiveness. The estimated data from reference 11 for discrete injection is plotted along with the VPCT data in figure 41. The value phi (ϕ) in the plot refers to the stalling flow coefficient as defined in reference 11. The lines shown are linear regression fits through all of the data for each system. The first observation is that the VPCT casing treatment does not follow the same characteristic trend in terms of injection velocity as the discrete injection system. Second, although there are considerably more data for the discrete injection systems, the trends indicate that the discrete injection is more effective by a factor of approximately two when posed in terms of injection velocity. For example, the VPCT provides a 3 percent improvement in for an injection velocity of approximately 45 percent of the tip velocity. At this same mass averaged injection velocity, the discrete system provides about 6 percent improvement in stalling flow coefficient, ϕ. Since these data are acquired on very different compression systems, it is possible this may affect the behavior trends from the characteristics shown. However, the performance advantage from discrete injection warrants investigation for noise impacts to a fan stage.

A summary plot of VPCT performance in terms of stall margin is shown in figure 42 where VPCT–1 shows the most stall margin improvement at 5.0 percent while VPCT–3 shows the lowest improvement at 3.3 percent. However, also shown in figure 42 are the noise impacts for the VPCT's, as available in reference 7 which indicate VPCT–2 was quieter, on an EPNdB basis, by 0.56 dB. This implies a trade exists between the stall margin desired and the acceptable noise impact since VPCT–1 was actually louder by 0.25 EPNdb. The greatest impact for the casing treatments tested was the stall margin improvement in the presence of inlet distortion. For these cases, the stall margin improvement was very large. Figure 43 summarizes the distorted inlet stall margin showing the largest improvement was 18.8 percent for VPCT–1 and the least was 13.3 percent for VPCT–7. However, VPCT–2, which was the quietest, also had an improvement over the smooth baseline of 18.2 percent, again indicating a trade between operability and noise exists. Finally, the efficiency impact is shown in figure 44 for each VPCT compared to the smooth case configuration. Unfortunately, although not unexpected, all of the VPCT's tested showed a loss in adiabatic efficiency when compared to the baseline. The minimum penalty was –2.1 percent for VPCT–2 and the largest was –3.6 percent for VPCT–4. Simply shutting the recirculation flow off does not recover the full efficiency penalty as the efficiency penalty for that case, VPCT–8, was –0.7 percent and with a decrease in stall margin of 1.0 percent. A more elegant solution for solving this problem would involve a sliding component to move axially and cover the slots at the casing wall, most likely for both the extraction location and the injection location.

Conclusions

A low tip speed, low-noise fan was tested for aerodynamic performance as part of a larger wind tunnel entry to investigate low noise concepts. The fan was designed for a cruise tip speed of 725 ft/sec with a pressure ratio of 1.294. The fan performance met design expectations but did have a significant instability near the design operating line. As part of the design evaluation, a novel casing treatment intended to improve operability was evaluated for noise and performance. Using this casing treatment, called Vaned Passage Casing Treatment, the stall performance improvement for the smooth inflow configurations varies among the casing treatments tested but all show a stall margin improvement over the baseline smooth case. The largest stall improvement for takeoff condition and a clean inlet, no inlet flow distortion, was 5 percent for VPCT–1 but with an efficiency penalty of 2.4 percent relative to the baseline smooth fan case. This large performance penalty underscores the need to use the recirculation only for

critical flight periods such as takeoff and provide a means of closing the slots at cruise operating conditions.

Perhaps of more notable interest, the overall noise levels of each casing treatment show it is possible to get either a slight noise penalty or a slight noise benefit, depending on the implementation of the casing treatment recirculation. The intriguing part of this is that one may be able to design a treatment that actually provides a stall margin improvement and a noise reduction benefit, albeit with an efficiency penalty over some mission segments. The optimal design would need to account for the impacts to each of these performance metrics and balance the design, as required for the application, between efficiency, noise generation, and stall margin. This optimization was not completed for any of the VPCT designs in this report.

Finally, the operating condition where the VPCT shows the largest benefit and greatest impact is demonstrated in the data acquired using a simulated inlet distortion. These cases show a dramatic improvement in stall margin for nearly all VPCT configurations tested. The stall margin improvement for the takeoff condition with inlet distortion was 18.8 percent for VPCT–1. This performance characteristic is important since the most benefit is provided during any critical operating conditions where distortion is encountered by the fan. This can drastically increase the safe operating range of a modern, high-bypass turbofan engine.

References

1. Kumasaka, Henry A., et al., "Definition of 1992 Technology Aircraft Noise Levels and the Methodology for Assessing Airplane Noise Impact of Component Noise Reduction Concepts," NASA CR 198298, 1996.
2. Groeneweg, John F., et al., "Turbomachinery Noise," Aeroacoustics of Flight Vehicles: Theory and Practice. Volume 1: Noise Sources, pp. 151–209, 1991. (See N92–10598 01–71)
3. Hobbs, David E., et al., Low-Noise Research Fan Stage Design. NASA CR–195382, 1995.
4. Jeracki, Robert J., "Comprehensive Report of Fan Performance From Duct Rake Instrumentation on 1.294 Pressure Ratio, 806 ft/sec Tip Speed Turbofan Simulator Models," NASA/TM—2005–213863, 2006.
5. Dittmar, James H., et al., "Some Acoustic Results from the Pratt and Whitney Advanced Ducted Propulsor – Fan 1," NASA TM 1999–209049, 1999.
6. Neubert, Robert, et al., Advanced Low-Noise Research Fan Stage Design. NASA CR 97–206308, 1997.
7. Elliott, David M., Dittmar, James, H., "Some Acoustic Results from the NASA/Pratt and Whitney Advanced Ducted Propulsor Model," AIAA 2000–0351, 38th Aerospace Sciences Meeting, Reno, Nevada, January 10–13, 2000.
8. Koff, S.G., Nikkanen, J.P., Mazzawy, R.S., "Rotor Case Treatment," U.S. Patent 5,308,225, May 3, 1994.
9. Hathaway, M. D., "Self-Recirculating Casing Treatment Concept for Enhanced Compressor Performance," ASME GT–2002–30368, ASME Turbo Expo 2002, Amsterdam, The Netherlands, June 3–6, 2002.
10. Suder, K.L., Hathaway, M.D., Thorp, S.A., Strazisar, A.J., and Bright, M.M., "Compressor Stability Enhancement Using Discrete Tip Injection," ASME Journal of Turbomachinery, vol. 123, no. 1, pp.14–23, January, 2001.
11. Strazisar, A.J., Bright, M.M., Thorp, S.A., Culley, Dennis E., Suder, K.L., "Compressor Stall Control Through Endwall Recirculation," ASME Paper no. GT2004–54295, IGTI Turbo Expo, Vienna, Austria.
12. Soeder, Ronald H., NASA Lewis 9- by15-Foot Low-Speed Wind Tunnel User Manual. NASA TM 106247, 1993.

TABLE 1.—FAN DESIGN PARAMETERS

Fan Parameter	P&W – NASA Low-Noise Fan 1	P&W – NASA Advanced Low-Noise Fan 2
Pressure Ratio		
SLTO	1.284	1.284
Cruise	1.294	1.294
Approach	1.077	1.077
Cutback	1.209	1.209
Corrected rpm		
SLTO	8,750	7,875
Cruise	8,400	7,557
Approach	5,000	4,425
Cutback	7,740	6,950
Corrected Tip Speed, ft/sec		
SLTO	840	756
Cruise	806	715
Approach	480	425
Cutback	743	667
Corrected W/A, lbm/sec ft^2		
SLTO	36.9	36.9
Cruise	42.5	42.5
Approach	22.7	22.7
Cutback	33.3	33.3
Bypass Ratio - Cruise	13.3	13.3
Blade Number	18	18
Vane Number	45	51
Hub/Tip	.426	.426
Diameter – LE, in.	22.0	22.0

TABLE 2.—VPCT TEST MATRIX CONFIGURATION SUMMARY

Item	Mass flow	Extraction	Injection	Aero Data*	Acoustic Data*
Smooth case	n/a	n/a	n/a	Yes	Yes
VPCT–1	Nominal	TE passage	LE passage	Yes	Yes
VPCT–2	Nominal	TE passage	Forward LE	Yes	Yes
VPCT–3	Nominal	Aft TE	LE passage	Yes	
VPCT–4	Max Flow	Aft TE	LE passage	Yes	Yes
VPCT–5	Nominal	Aft TE	Forward LE	Yes	Yes
VPCT–6	Max Flow	Aft TE	Forward LE	No	Yes
VPCT–7	Reduced Flow	TE passage	LE passage	Yes	
VPCT–8	OFF	TE passage	LE passage	Yes	

*Inconsistent type and quantity of data may be available between configurations depending on test goals.

TABLE 3.—VPCT PERFORMANCE DATA SUMMARY TABLE

Configuration	Stall margin (%)	Delta stall margin (%)	Delta phi (%)	Operating line efficiency (%)	Delta efficiency (%)	Takeoff delta EPNdB
Baseline	227			936		
VPCT–1 passage inj and extr	27.7	5.0	4.6	91.2	–2.4	0.25
VPCT–2 fwd inj	26.2	3.5	3.1	91.6	–2.1	–0.56
VPCT–3 aft extr	26.0	3.3	3.8	90.1	–3.6	n/a
VPCT–4 aft extr, max flow	n/a	n/a	n/a	90.2	–3.5	0.21
VPCT–5 fwd inj and aft extr	26.5	3.8	3.0	91.5	–2.2	–0.47
VPCT–6 fwd inj aft extr max flow	n/a	n/a	n/a	n/a	n/a	–0.5
VPCT–7 (–1 with reduced flow)	26.6	3.9	3.6	92.1	–1.5	n/a
VPCT–8 (recirc off)	21.7	–1.0	–0.8	92.9	–0.7	n/a

TABLE 4.—VPCT STALL PERFORMANCE SUMMARY WITH INLET DISTORTION

| Configuration with distortion iscreen in inlet	Stall margin (%)	Delta stall margin (%)	Delta phi (%)	Takeoff delta EPNcIB
Baseline	5.2			
VPCT–1 passage inj and extr	24.0	18.8	13.8	0.25
VPCT–2 fwd inj	23.3	18.2	12.4	–0.56
VPCT–3 aft extr	20.0	14.9	11.9	n/a
VPCT–4 aft extr, max flow	n/a	n/a	n/a	0.21
VPCT–5 fwd inj and aft extr	19.3	14.1	10.5	–0.47
VPCT–6 fwd inj aft extr max flow	n/a	n/a	n/a	–0.5
VPCT–7 (–1 with reduced flow)	18.5	13.3	10.8	n/a
VPCT–8 (recirc off)	n/a	n/a	n/a	n/a
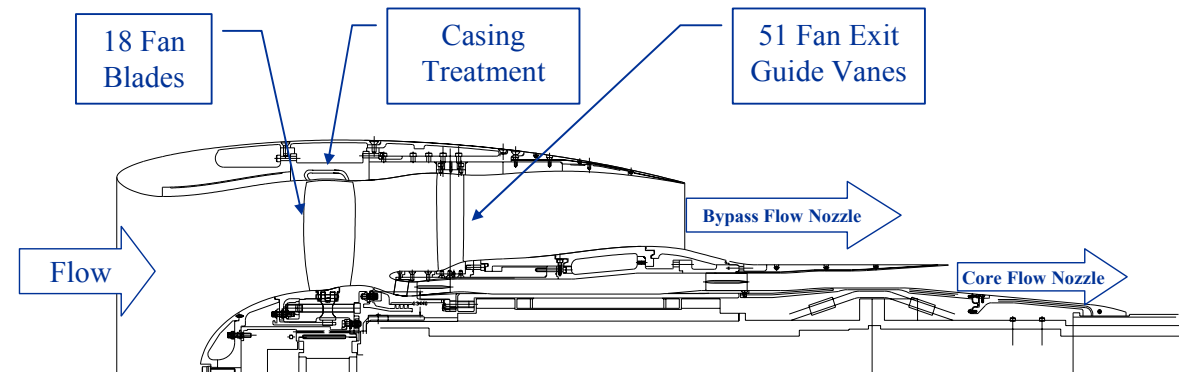
Figure 1.—Fan 2 cross section.
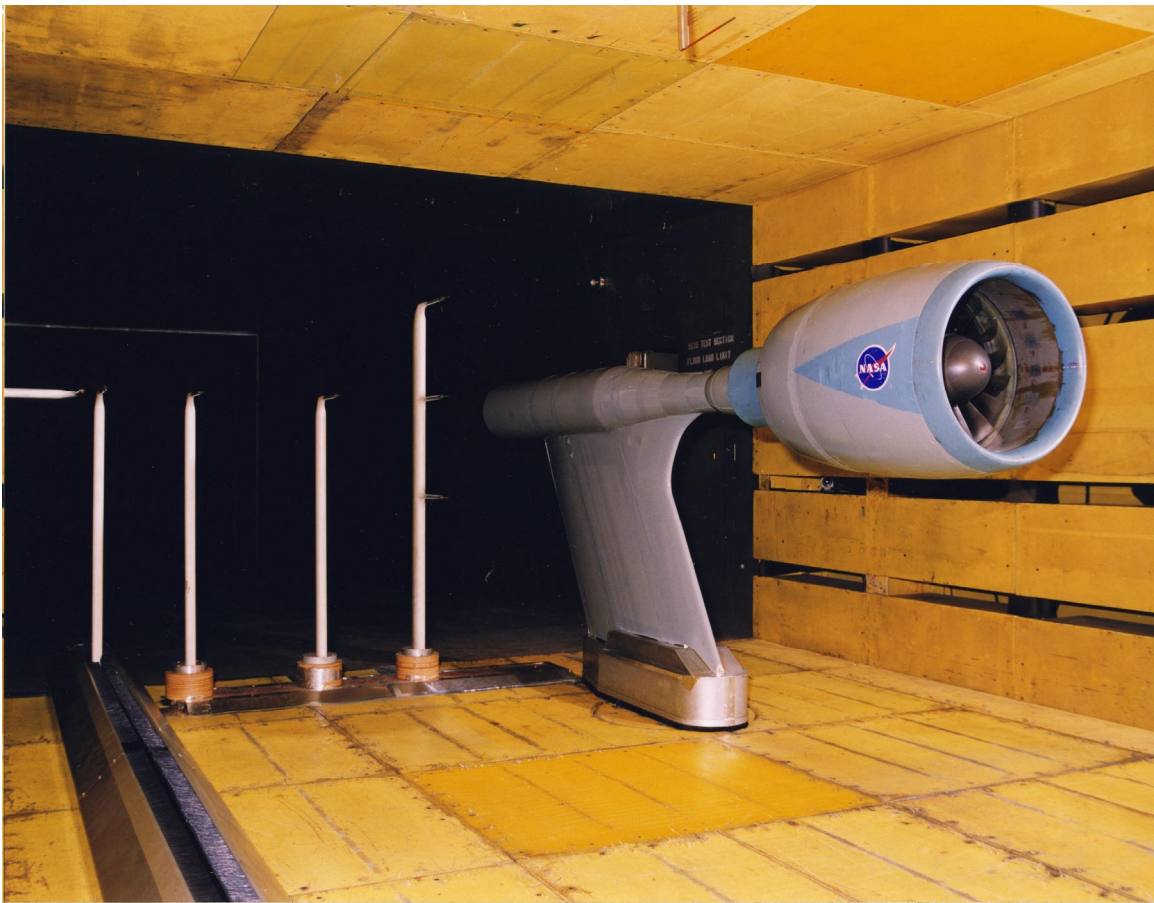
Figure 2.—Acoustic testing configuration.

Figure 3.—Performance configuration.
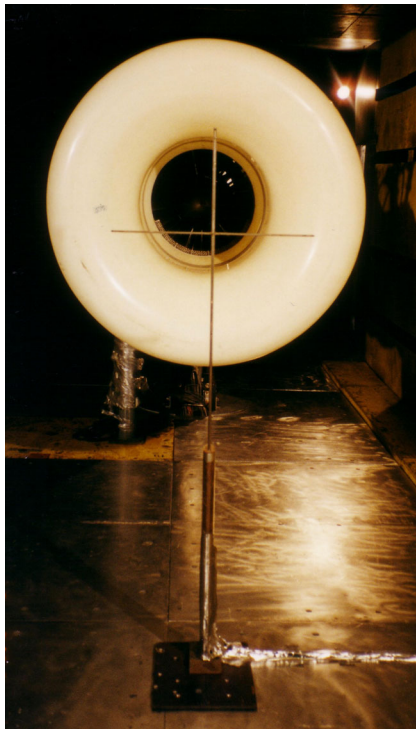
○ - Total Pressure

◇ - Total Temperature

◎ - RTD Temperature
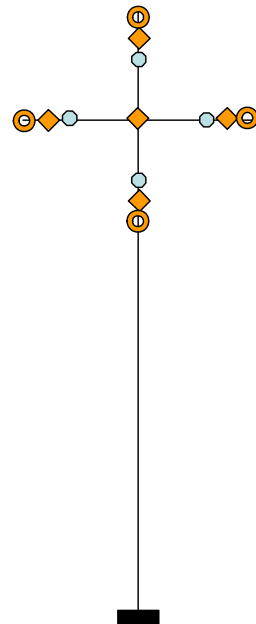
Figure 4.—Cruciform rake and associated instrumentation.
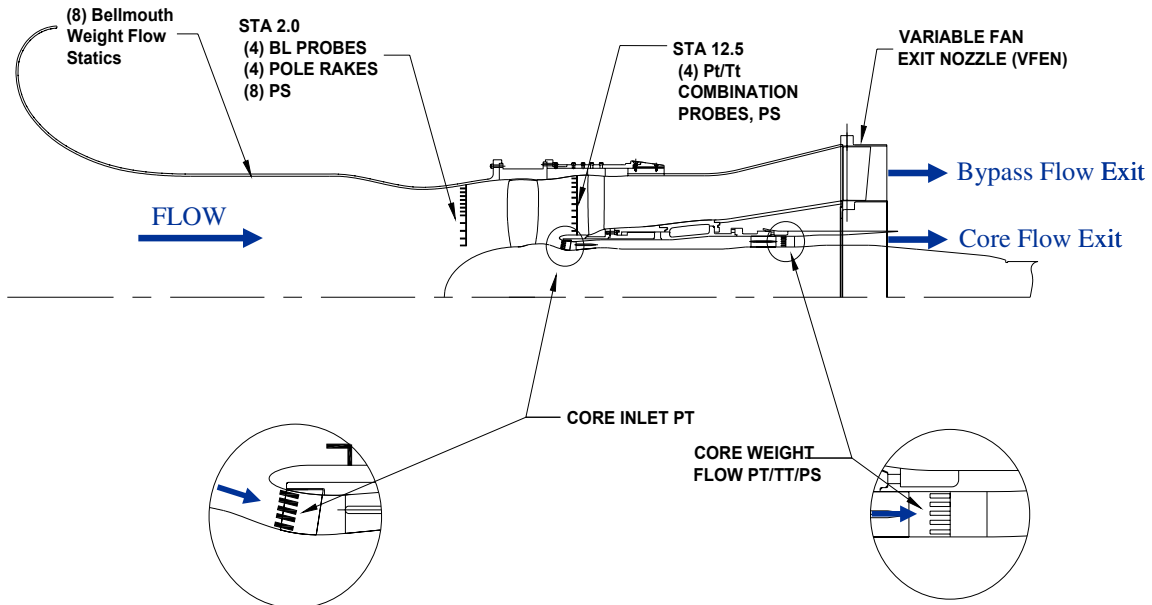
Figure 5.—Performance configuration cross section.
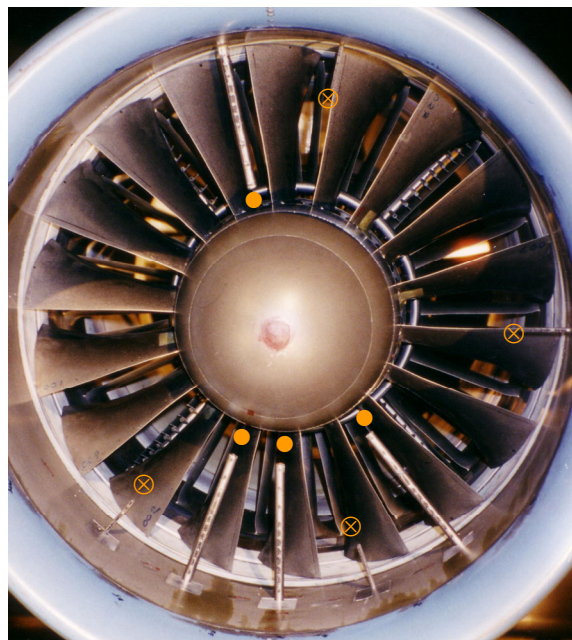
Pole Rakes ●		Boundary Layer Rakes ⊗	
Angle, (CCW from TDC viewed from front) 12°, 160°, 180°, 220°		Angle, (CCW from TDC viewed from front) 140°, 200°, 270°, 348°	
Radius, in.		Radius, in.	
5.464		8.929	
6.186		9.217	
6.908		9.578	
7.630		9.794	
7.990		10.083	
8.351		10.191	
8.712		10.300	
9.073		10.372	
9.434		10.444	
9.794			
10.155			

Figure 6.—Representative inlet rake layout at STA 2.0 (STA 164.44 in.).

STA 12.5 Combination PT & TT Rakes, Typical 4 places

Core Instrumentation PT & TT, Typical 2 places

STA 12.5	Core Instrumentation		
Rakes @ 46°,132°,228°,314°	Radius, in.	Angles* PT	Angles* TT
Radius, in.	4.601	80°, 350°	85°, 355°
6.204	4.758	70°, 340°	75°, 345°
6.924	4.916	60°, 330°	65°, 335°
7.577	5.073	50°, 320°	55°, 325°
8.177	5.231	40°, 310°	45°, 315°
8.737			
9.263			
9.760			
10.233			
10.685			
11.119			

All angles CCW from TDC fwd looking aft
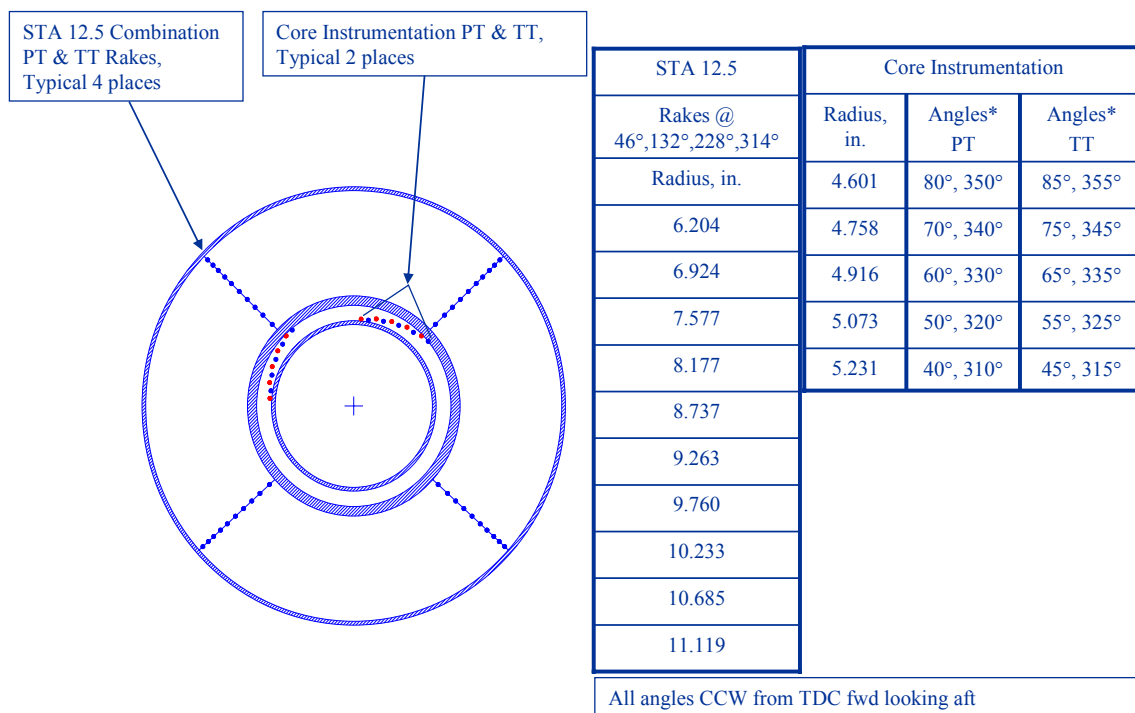
Figure 7.—STA 12.5 and core instrumentation radial and circumferential locations.
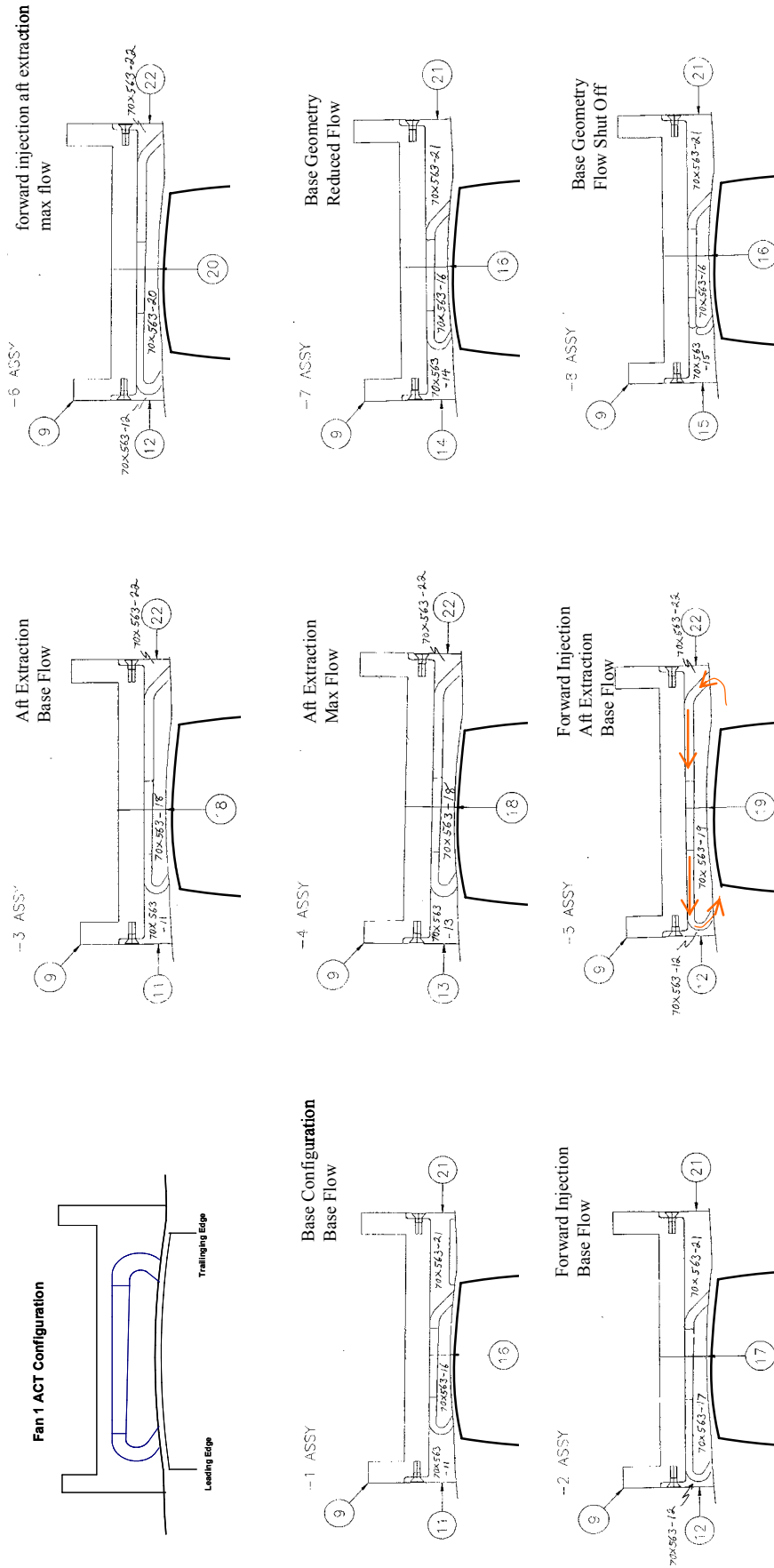
Figure 8.—Casing treatment configurations.
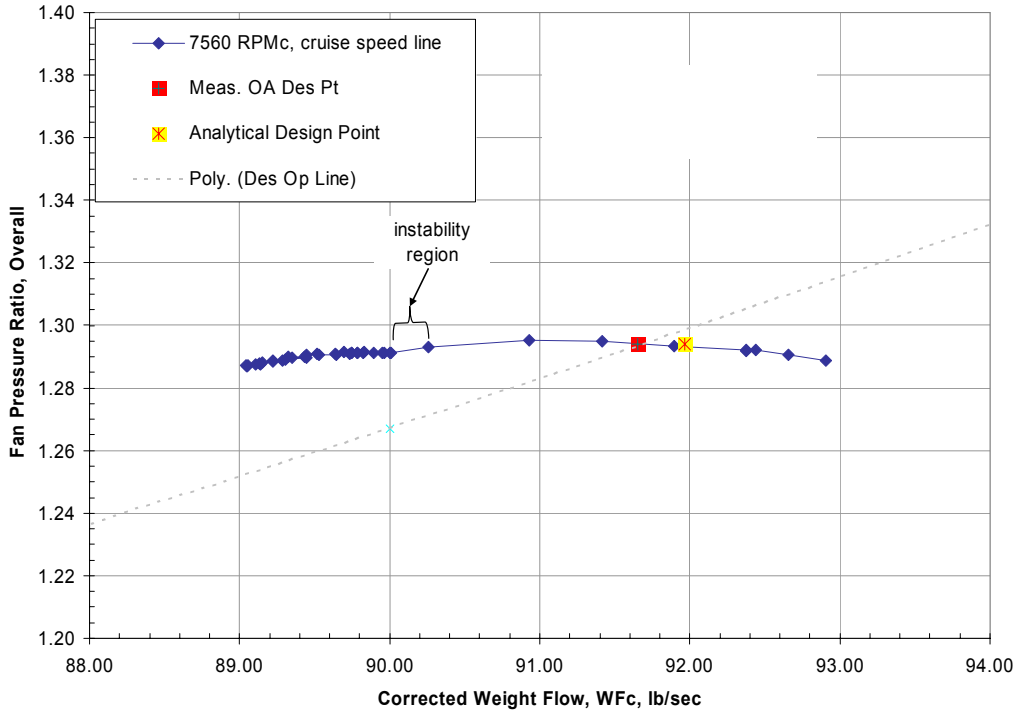
Figure 9.—Fan 2, cruise condition, 7560 rpmc speed line.
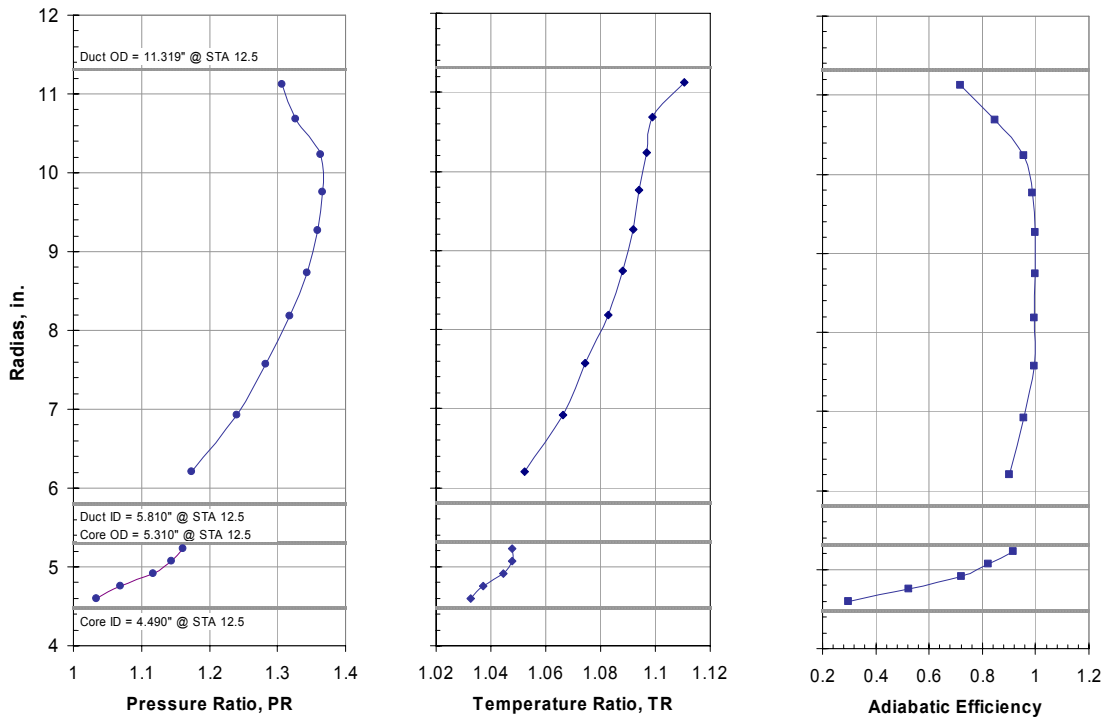
Figure 10.—Pressure, temperature, and adiabatic efficiency profiles for cruise.
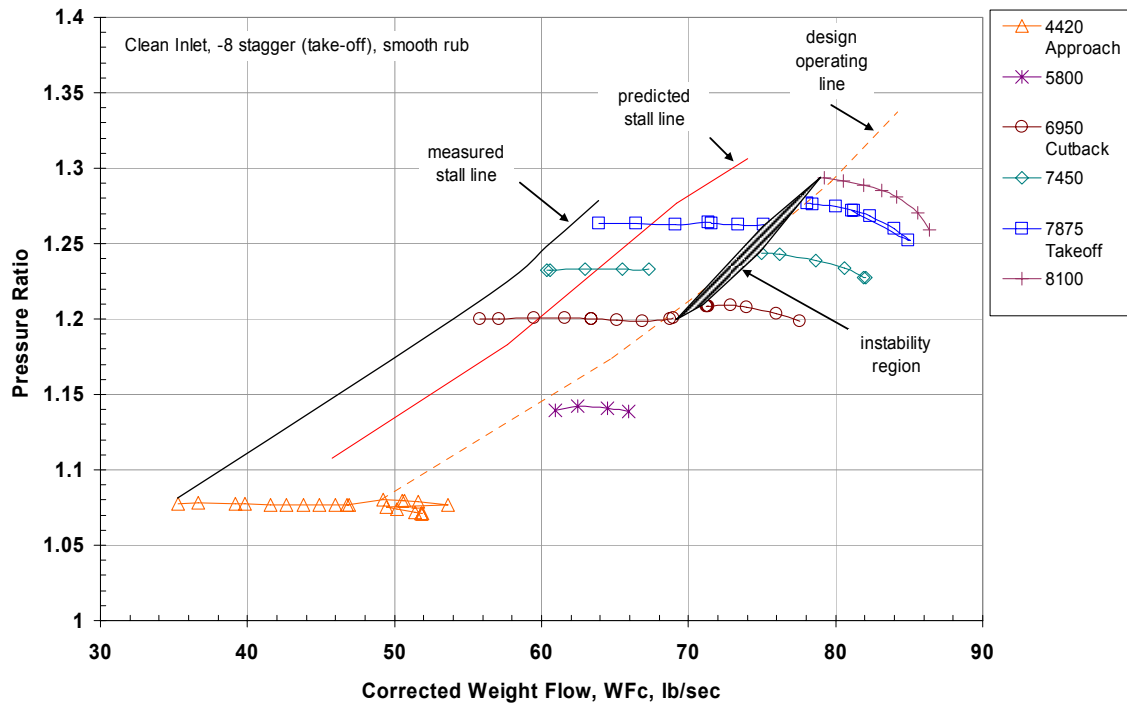
Figure 11.—Baseline Fan 2 pressure ratio versus corrected weight flow.
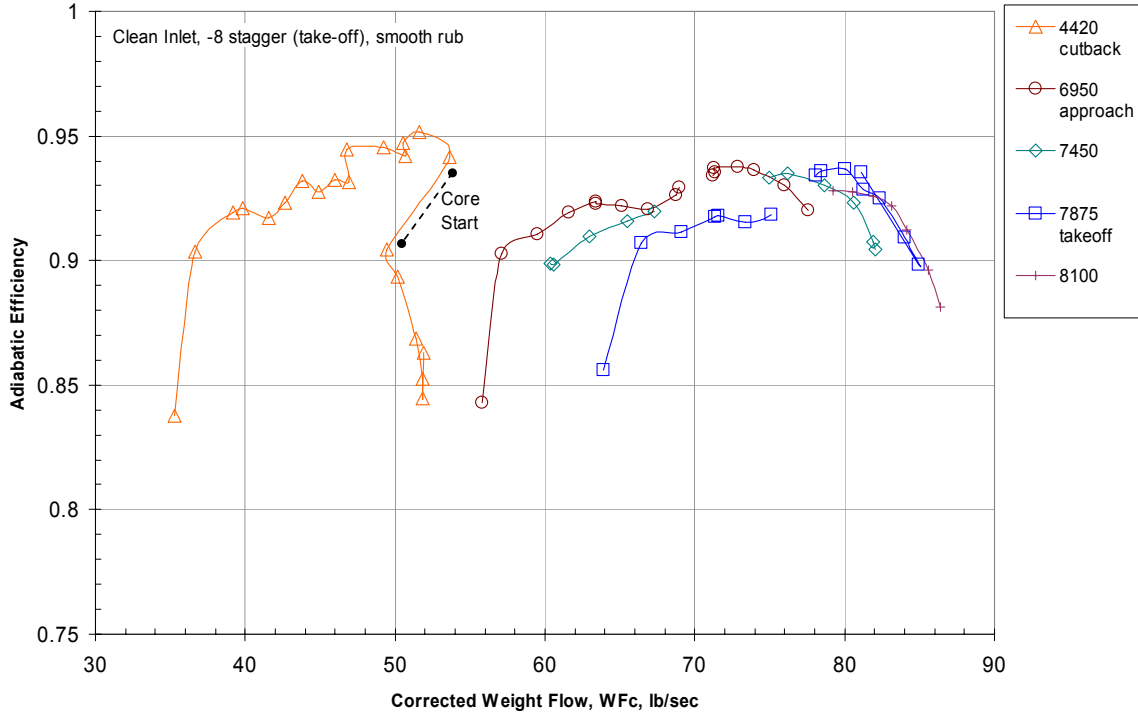
Figure 12.—Baseline Fan 2 average adiabatic efficiency versus corrected weight flow.
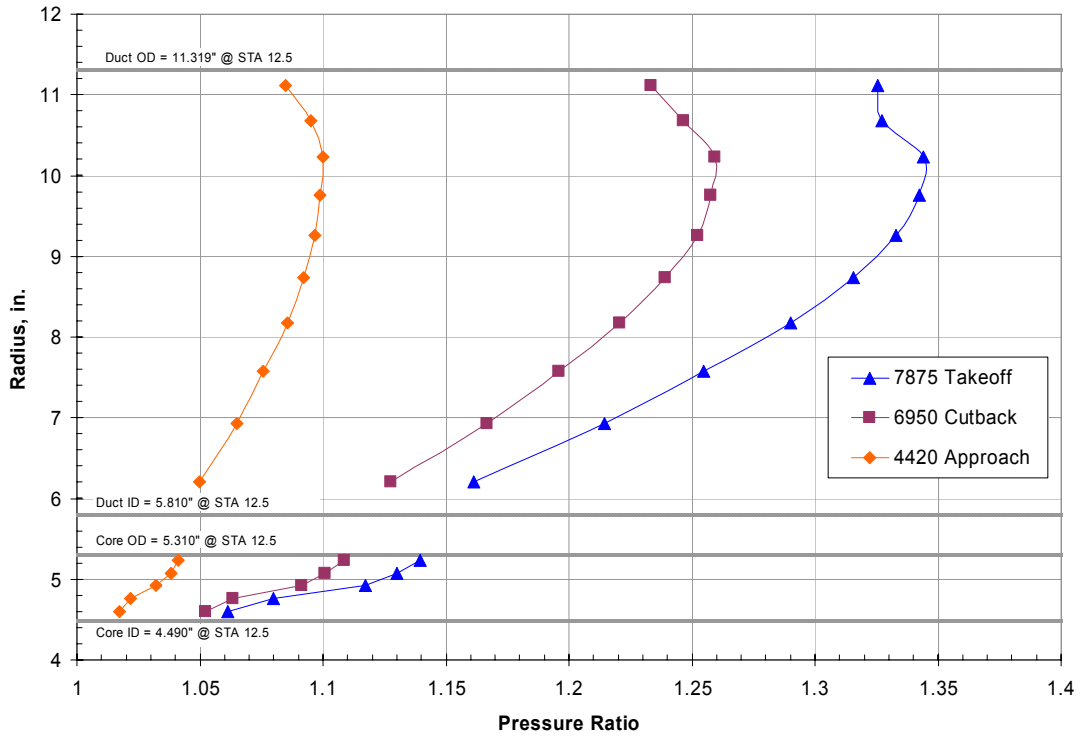
Figure 13.—Baseline pressure profile, bypass and core, on operating line.
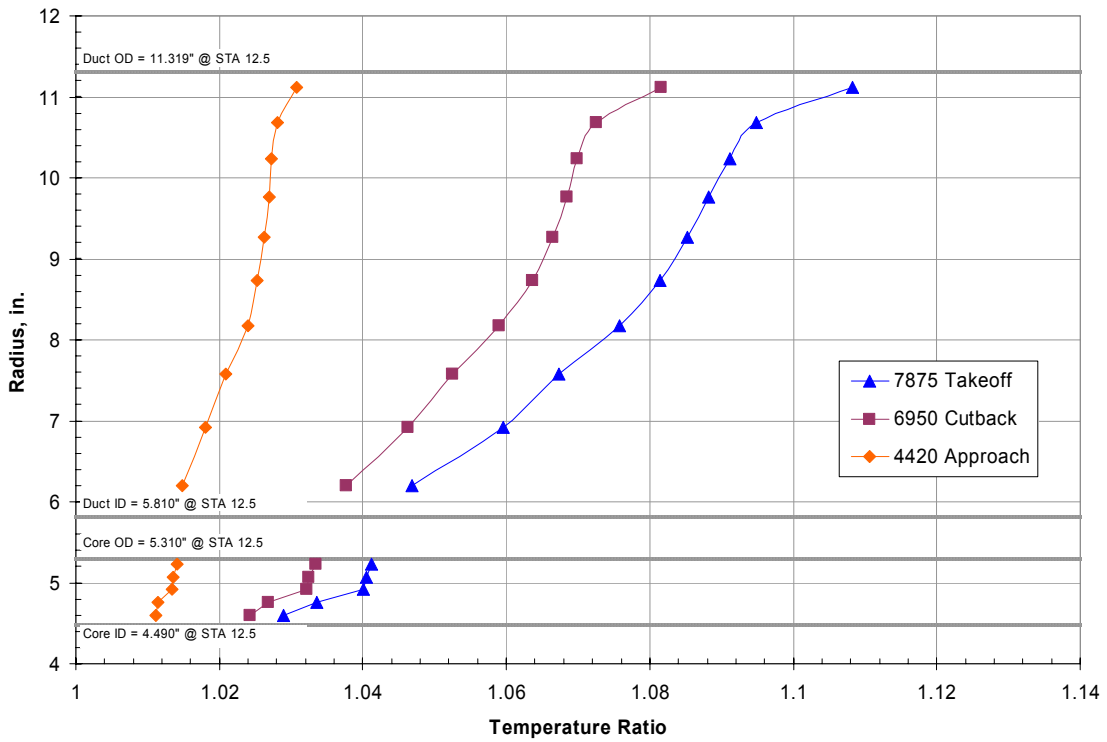
Figure 14.—Baseline temperature profile, bypass and core, on operating line.
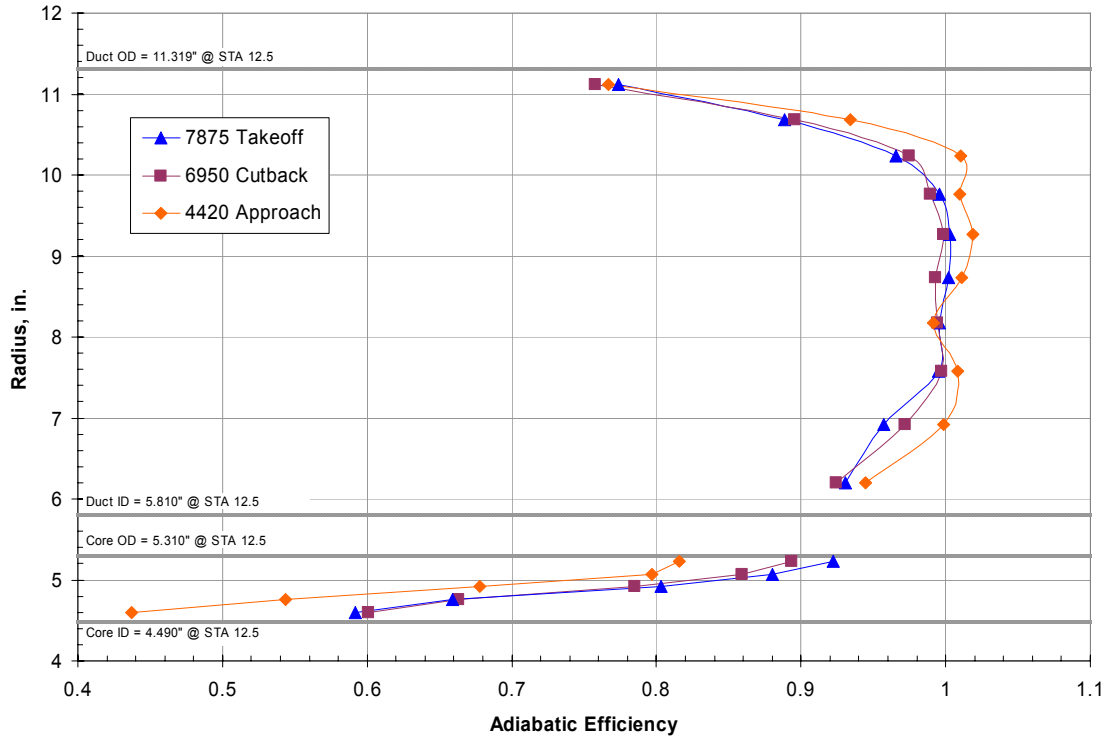
Figure 15.—Baseline efficiency profile, bypass and core, on operating line.
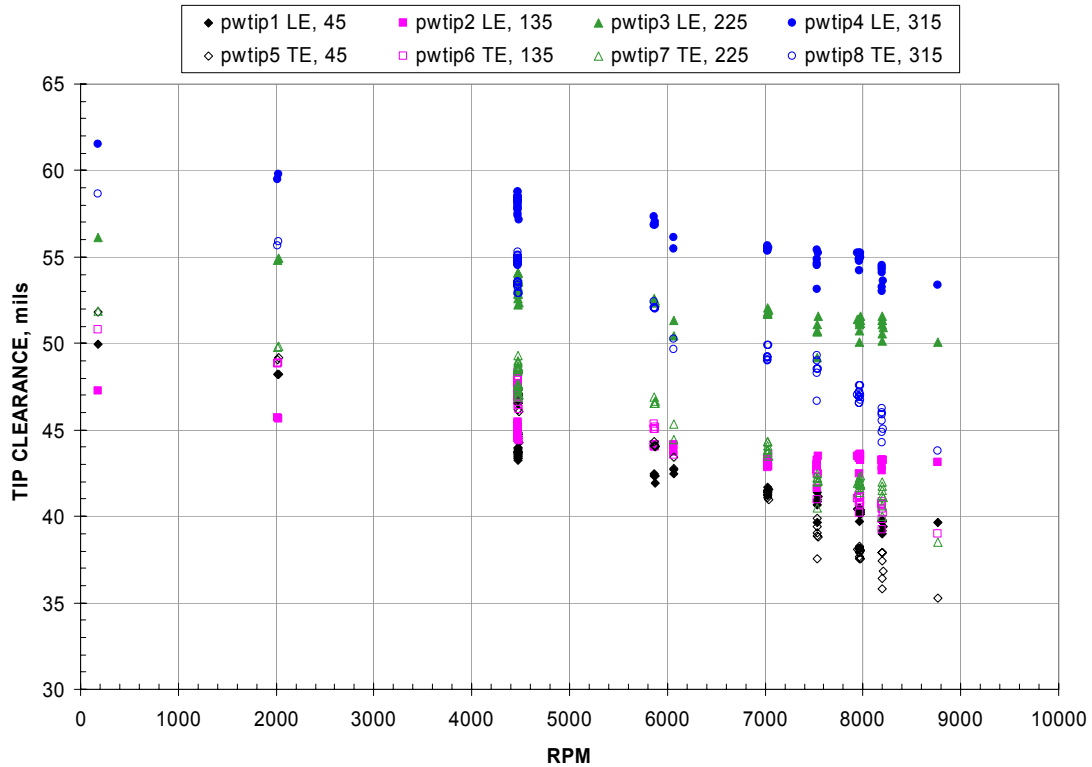
Figure 16.—Fan 2 measured tip clearance.
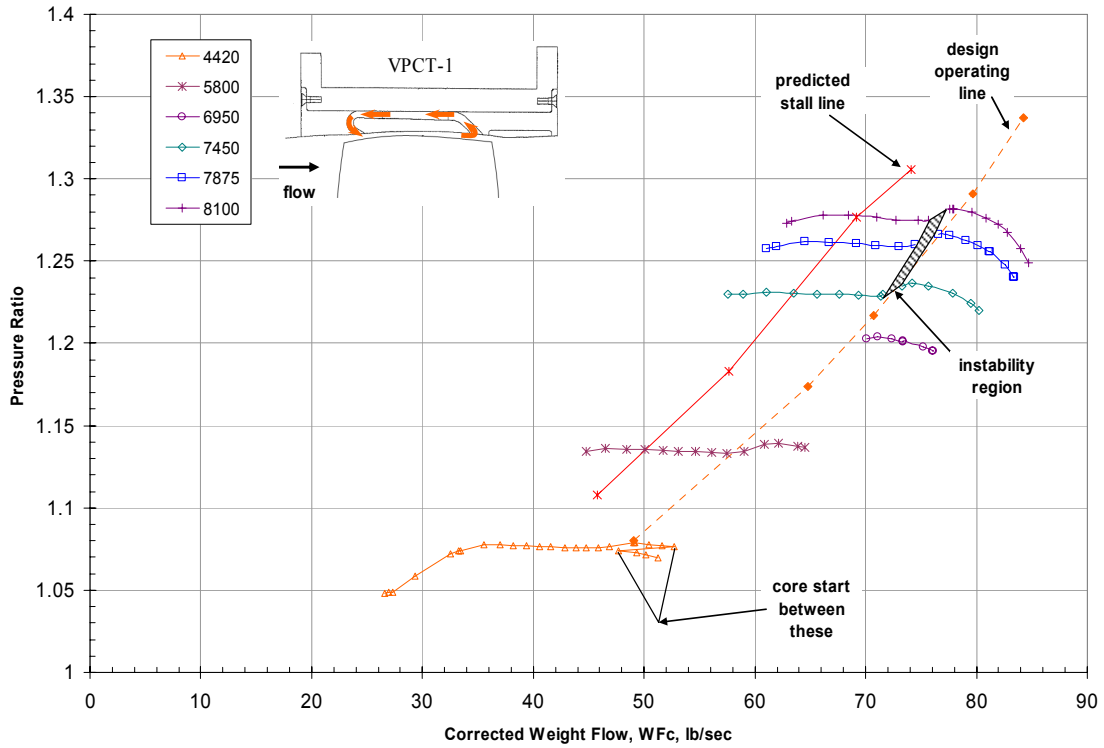
Figure 17.—Fan map with VPCT–1.
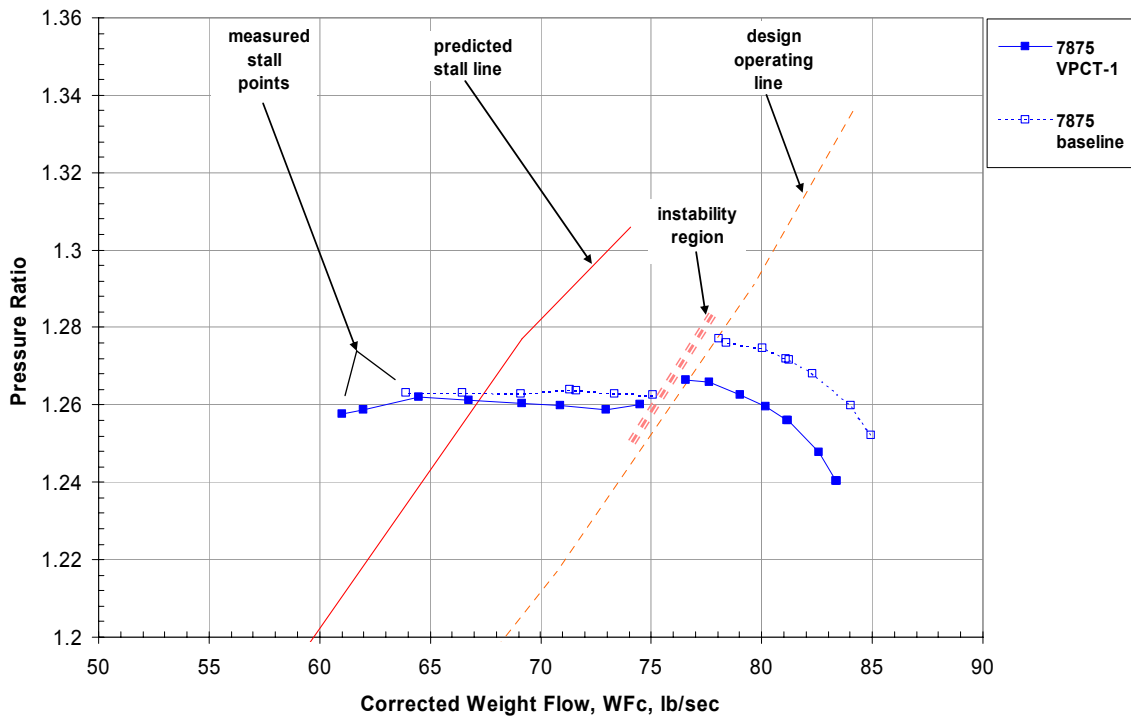
Figure 18.—VPCT–1 and baseline takeoff speed lines.
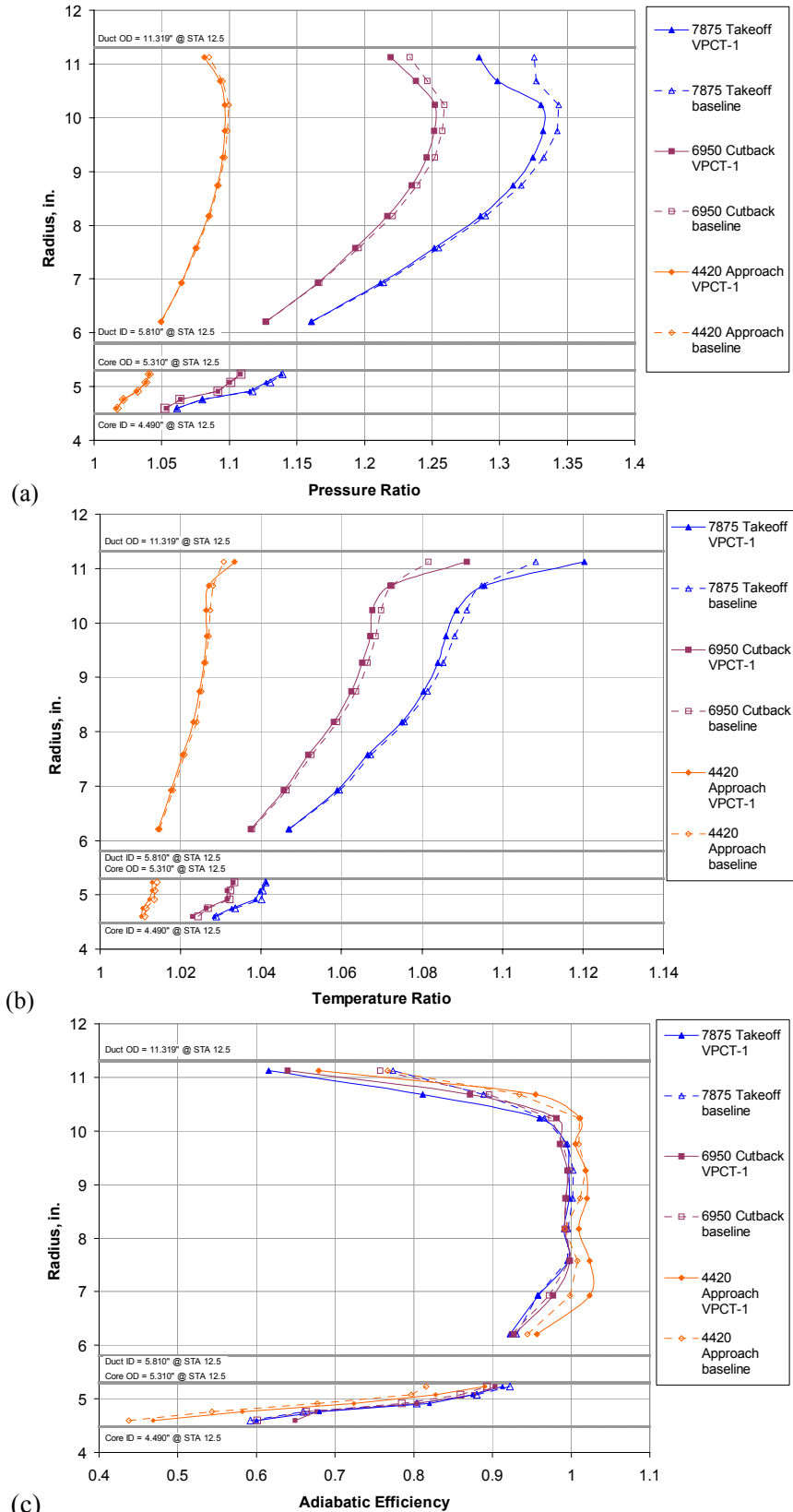
Figure 19.—Radial profiles of (a) pressure ratio, (b) temperature ratio, and (c) adiabatic efficiency for VPCT–1; bypass and core, on operating line.
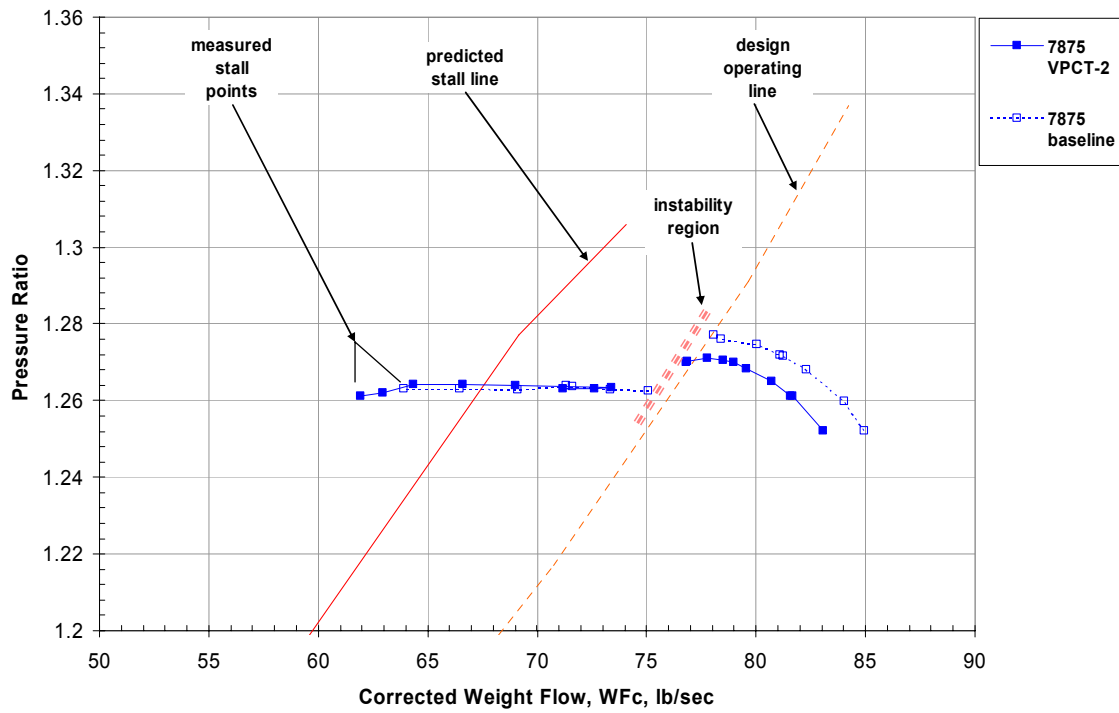
Figure 20.—VPCT–2 and baseline takeoff speed lines.
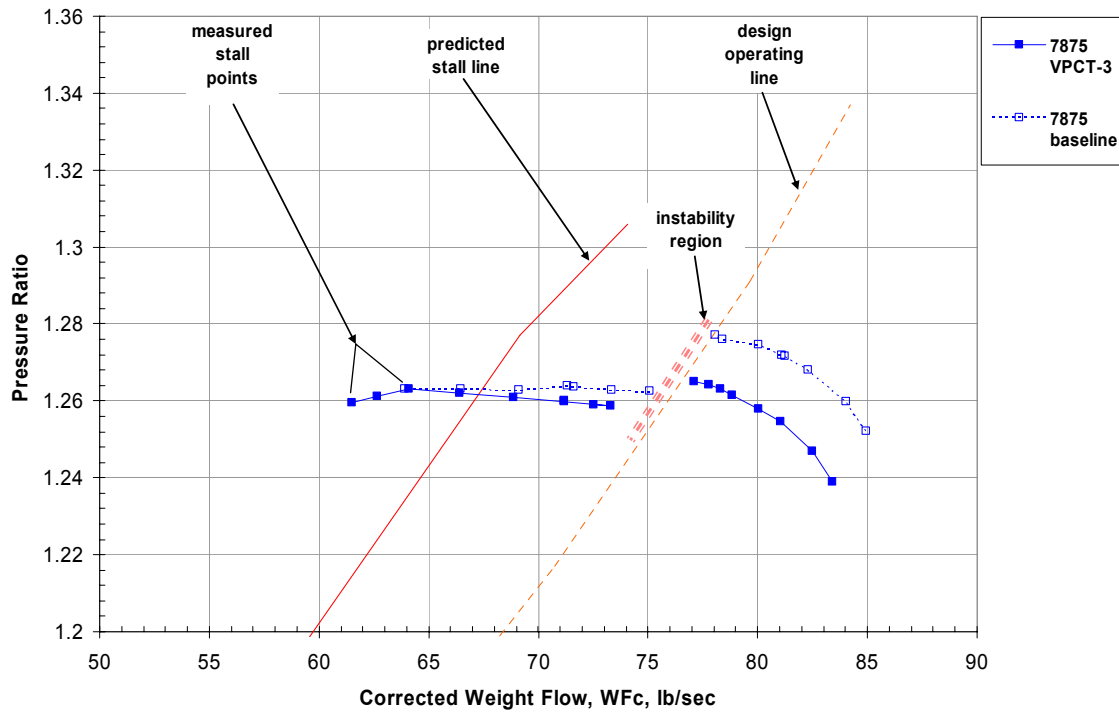
Figure 21.—VPCT–3 and baseline takeoff speed lines.
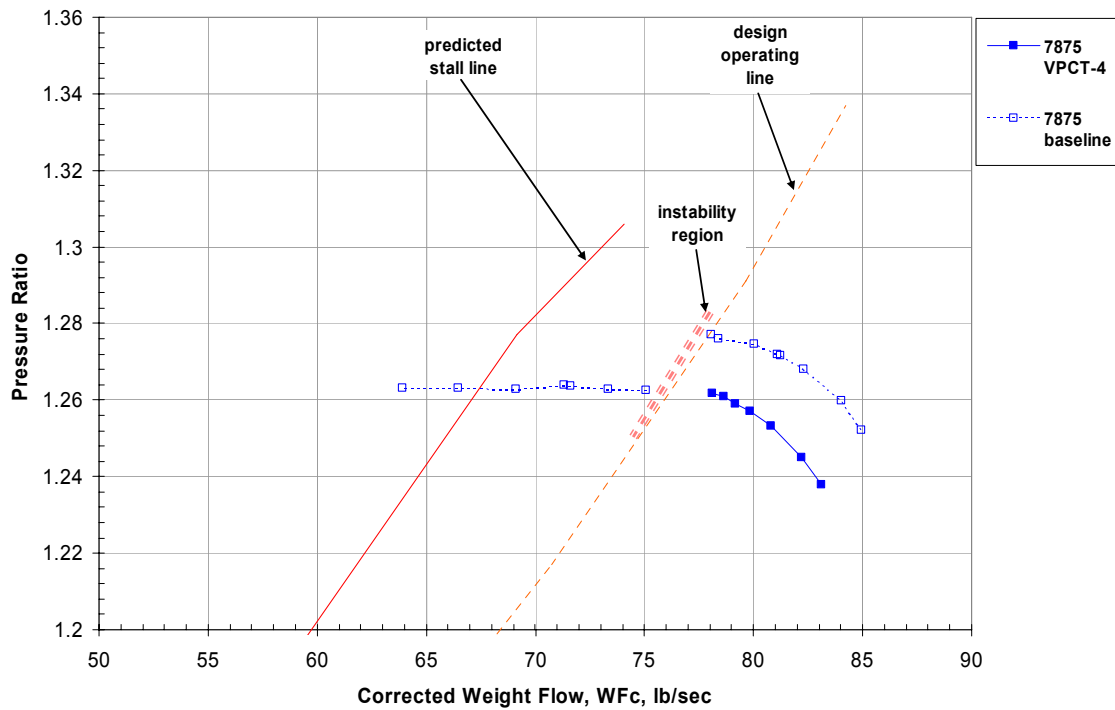
Figure 22.—VPCT–4 and baseline takeoff speed lines.
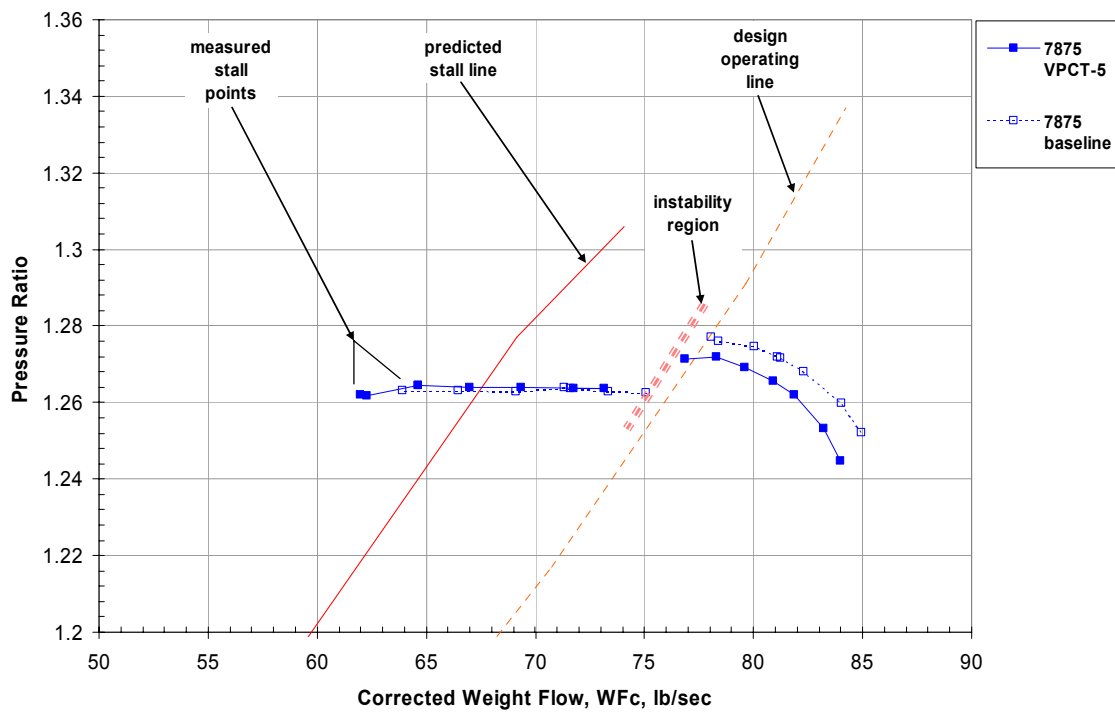
Figure 23.—VPCT–5 and baseline takeoff speed lines.
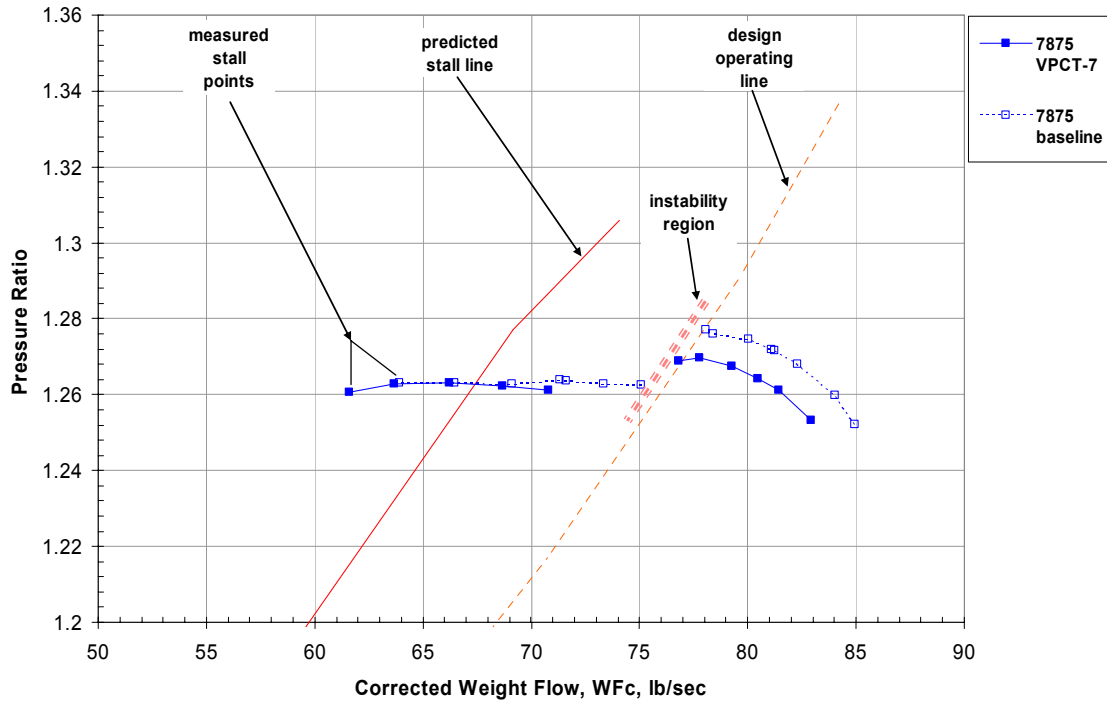
Figure 24.—VPCT–7 and baseline takeoff speed lines.
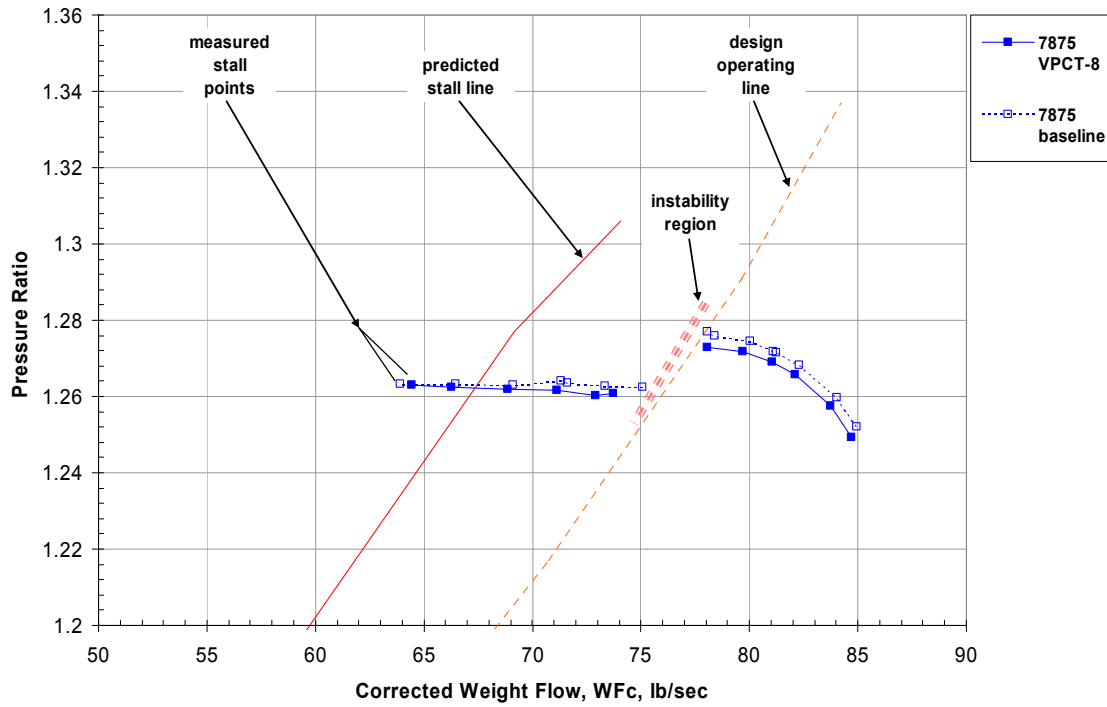
Figure 25.—VPCT–8 and baseline takeoff speed lines.
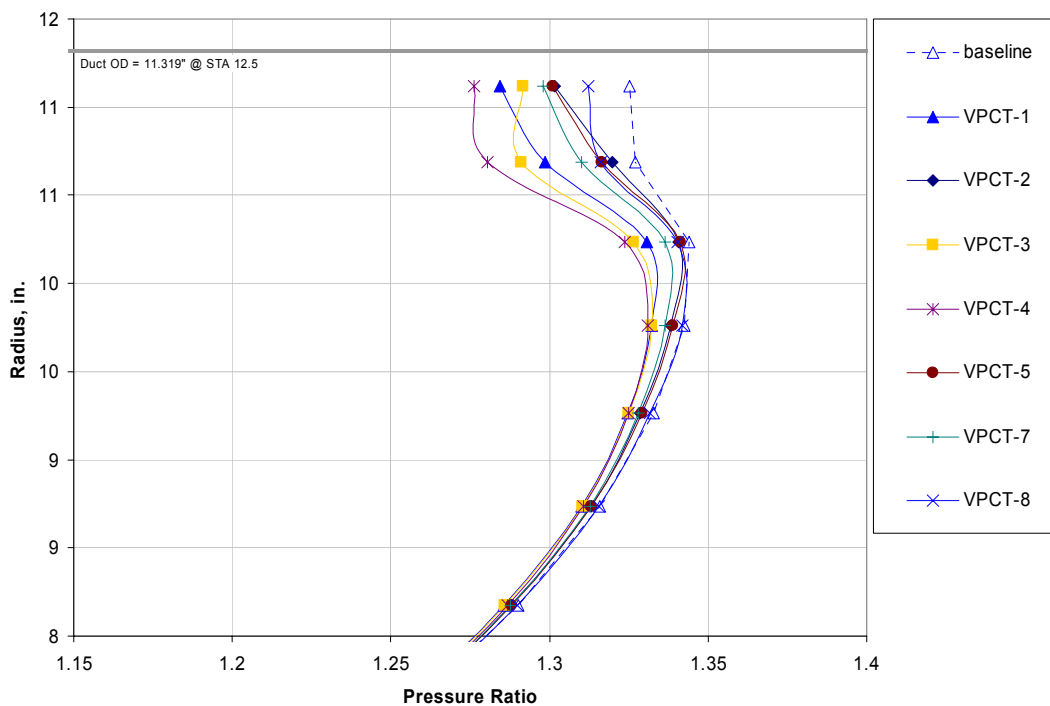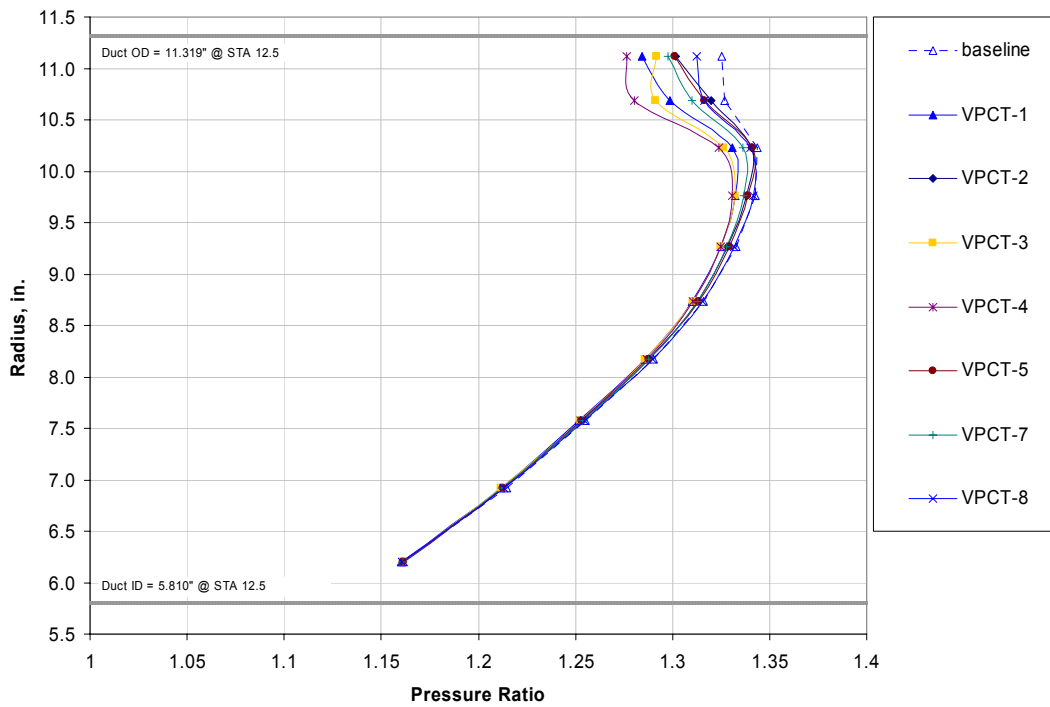
Figure 26.—(a) Total pressure radial profile all VPCT configurations, (b) Total pressure radial profile all VPCT configurations zoomed.
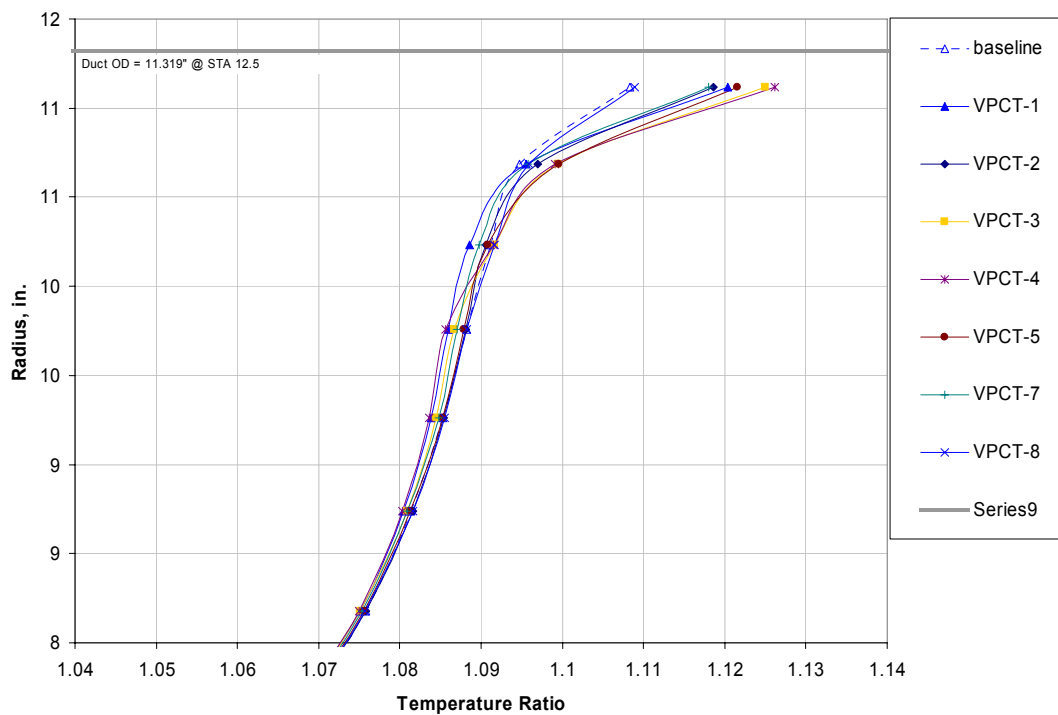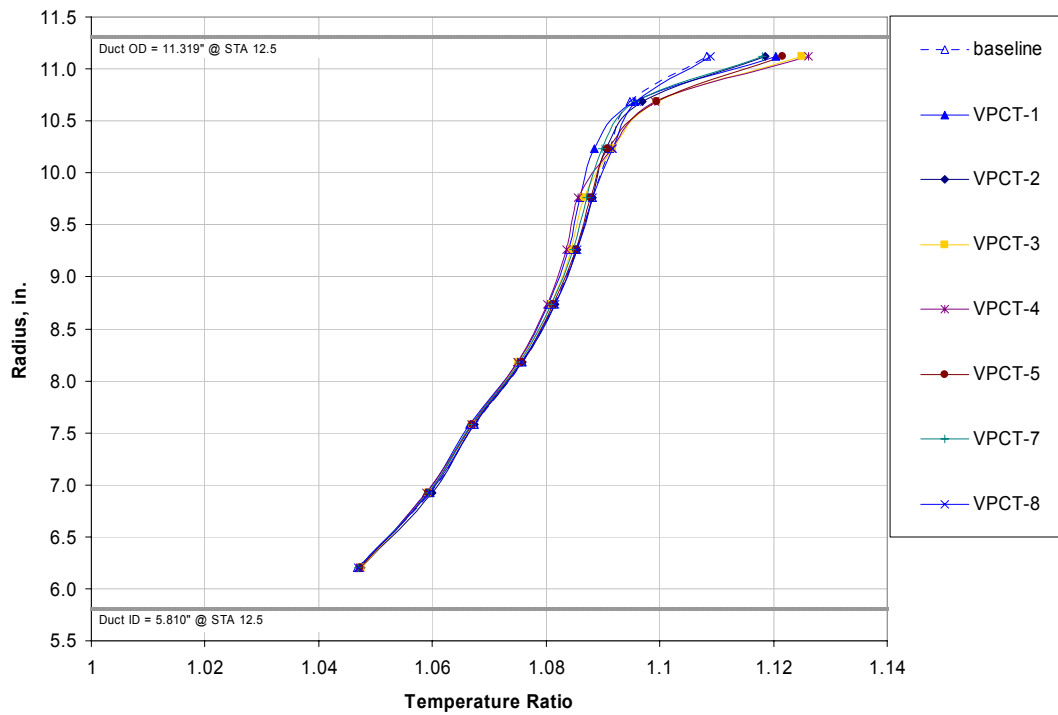
Figure 27.—(a) total temperature radial profile all VPCT configurations, (b) Total
temperature radial profile all VPCT configurations zoomed.
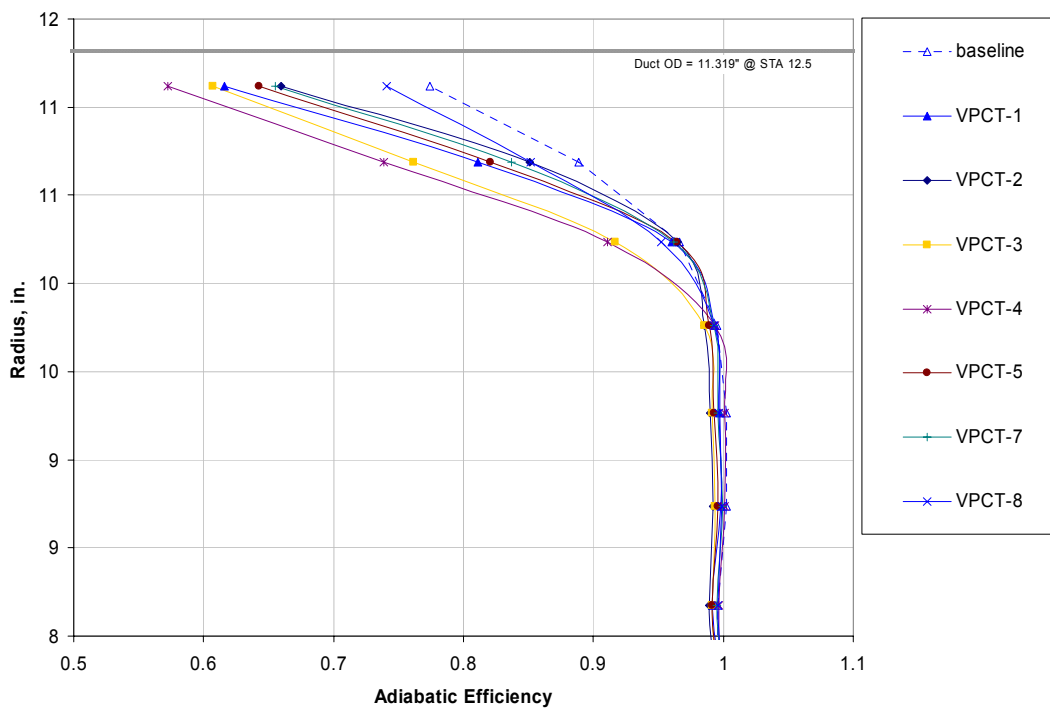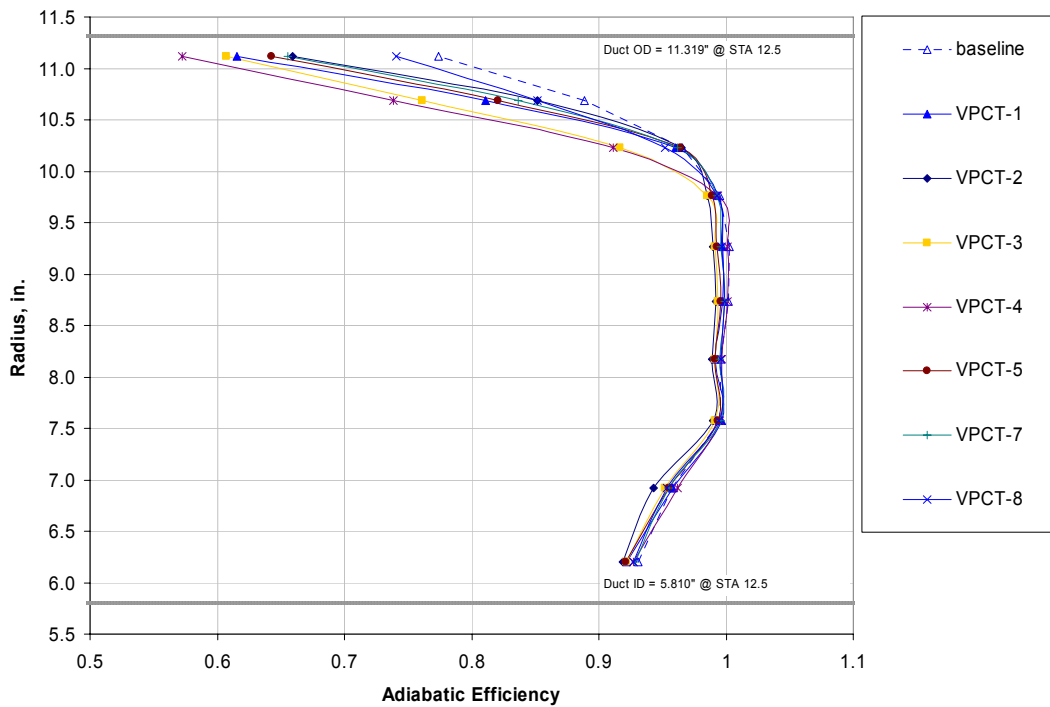
Figure 28.—(a) Adiabatic efficiency radial profile all VPCT configurations, (b) Adiabatic efficiency radial profile all VPCT configurations zoomed.
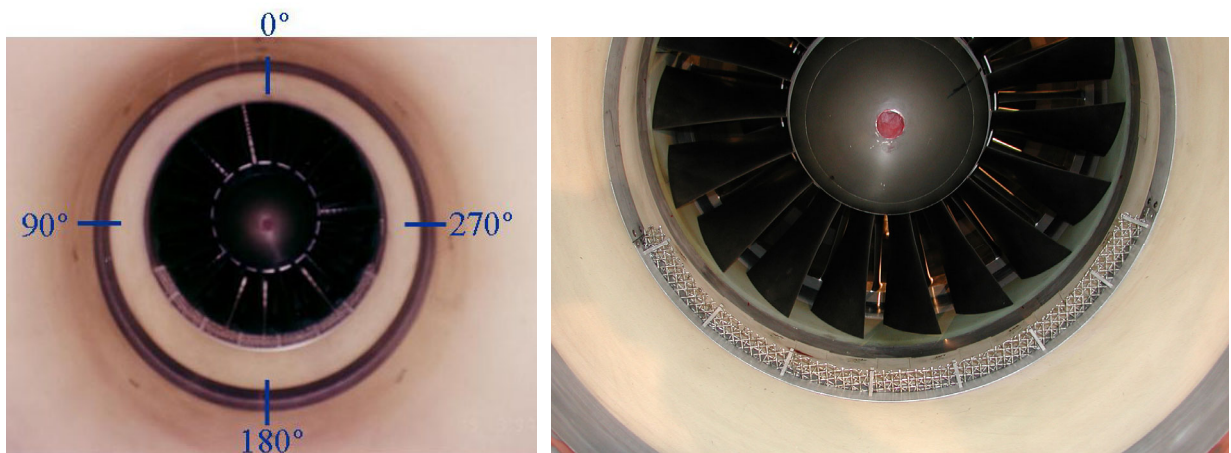
Figure 29.—Distortion screen mounted in bell mouth inlet.
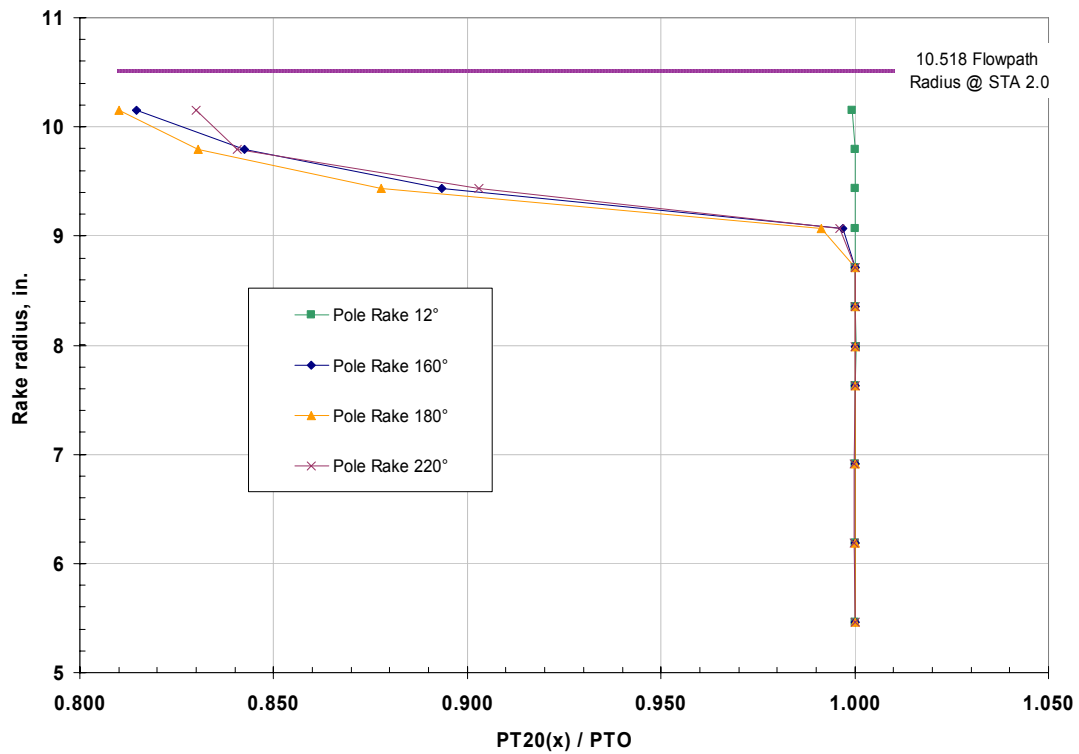
Figure 30.—Inlet Distortion measured using pole rakes at station 164.44 in.
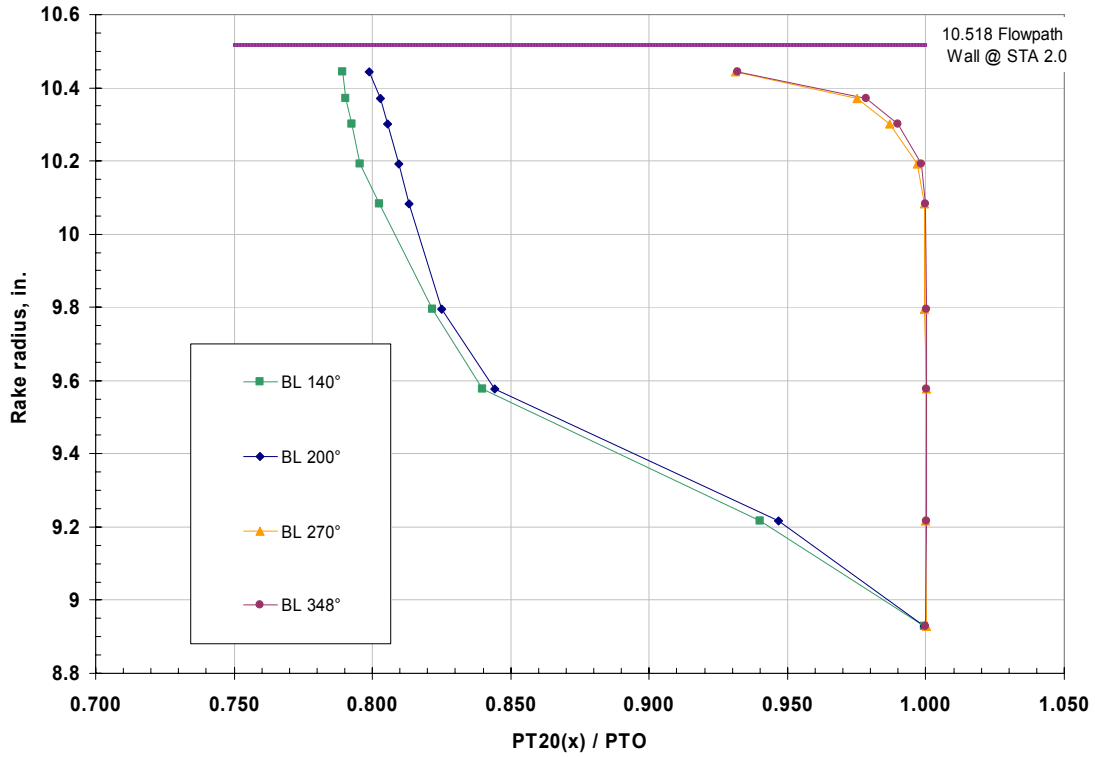
Figure 31.—Distortion measured using boundary layer rakes at STA 164.44 in.
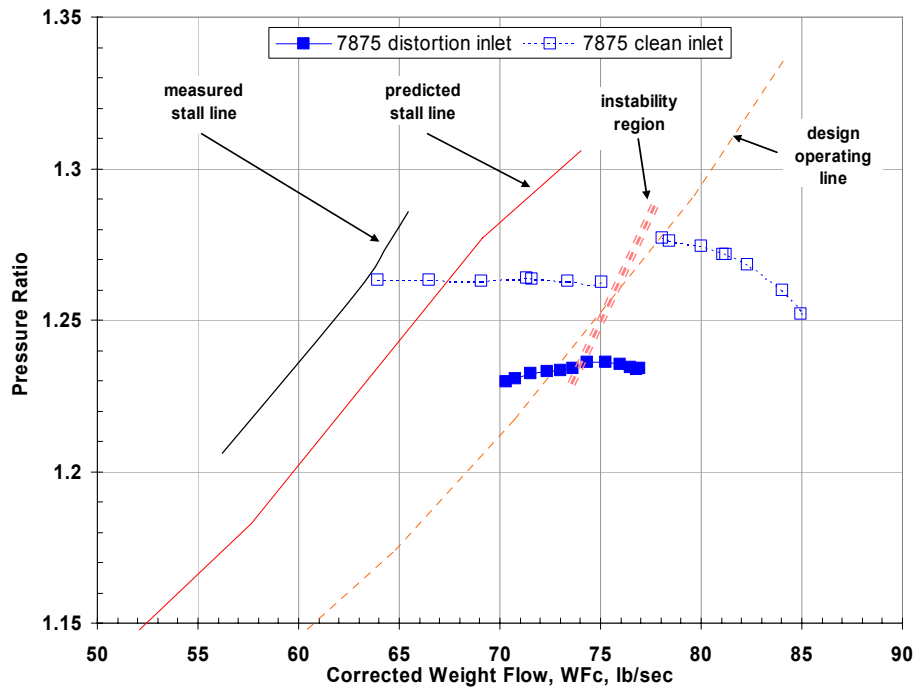
Figure 32.—Takeoff speed line with inlet distortion and smooth case
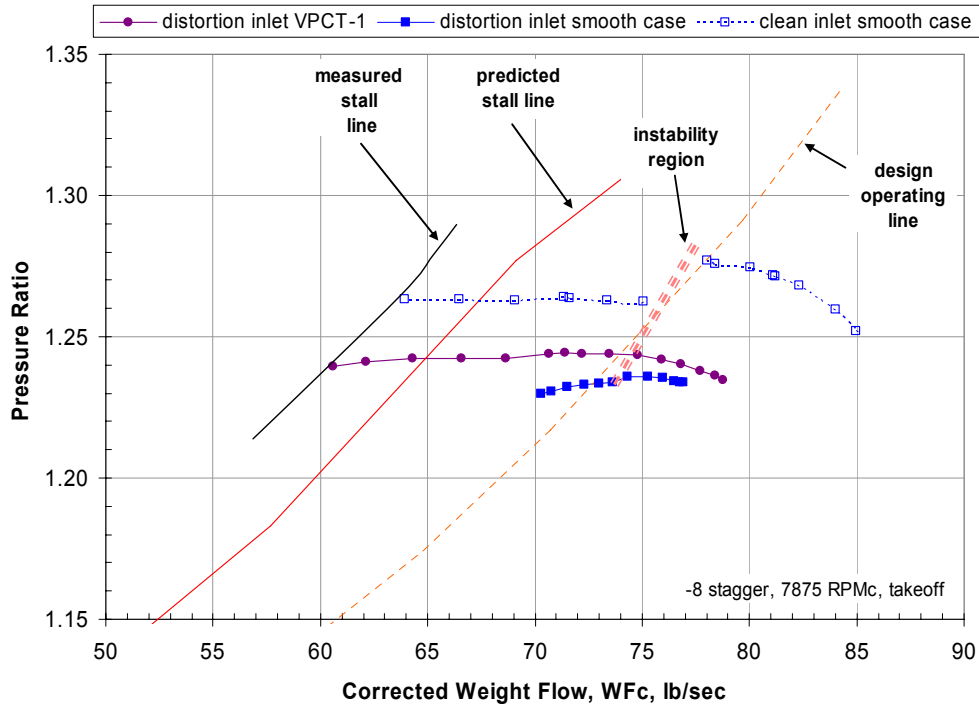
Figure 33.—Fan 2 pressure ratio versus corrected weight flow, with inlet distortion and VPCT–1.
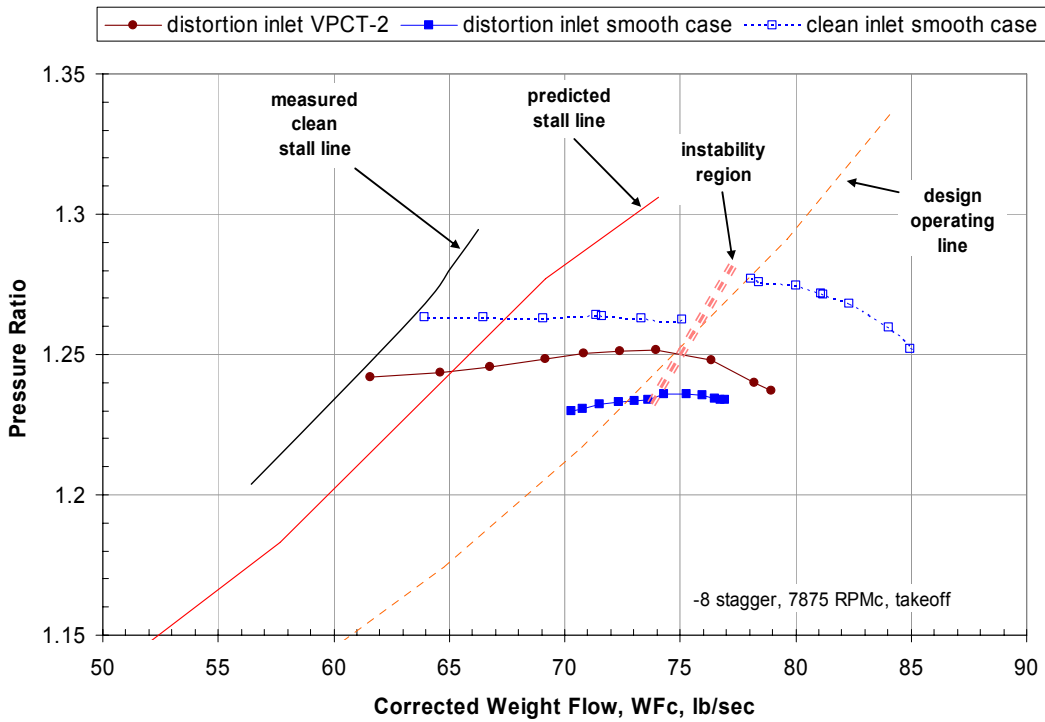
Figure 34.—Fan 2 pressure ratio versus corrected weight flow, with inlet distortion and VPCT–2.
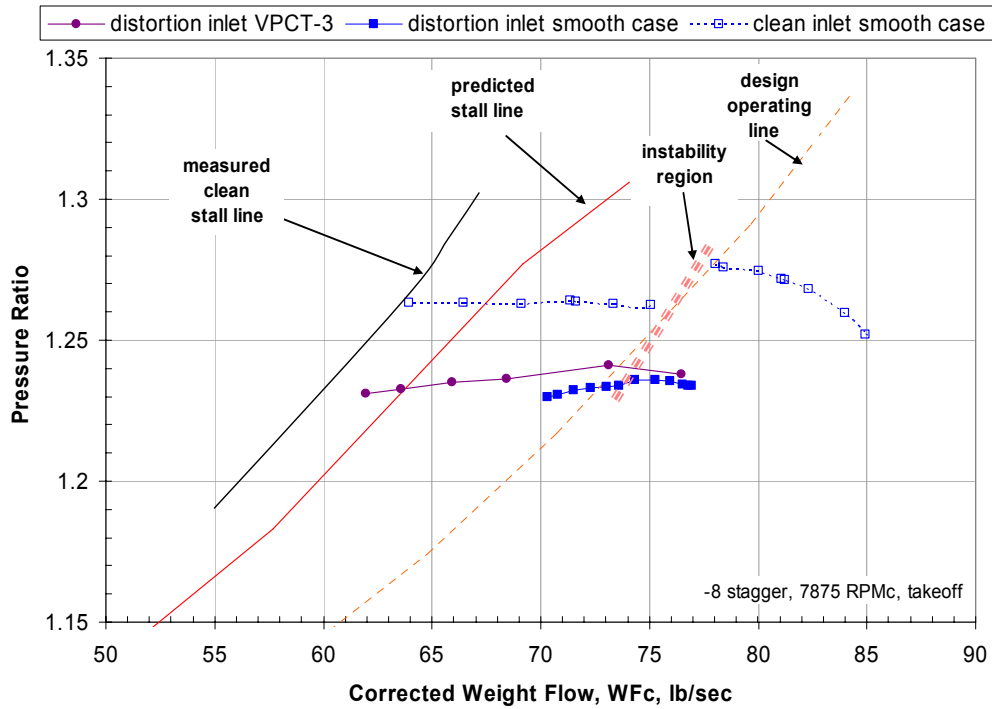
Figure 35.—Fan 2 pressure ratio versus corrected weight flow, with inlet distortion and VPCT–3.
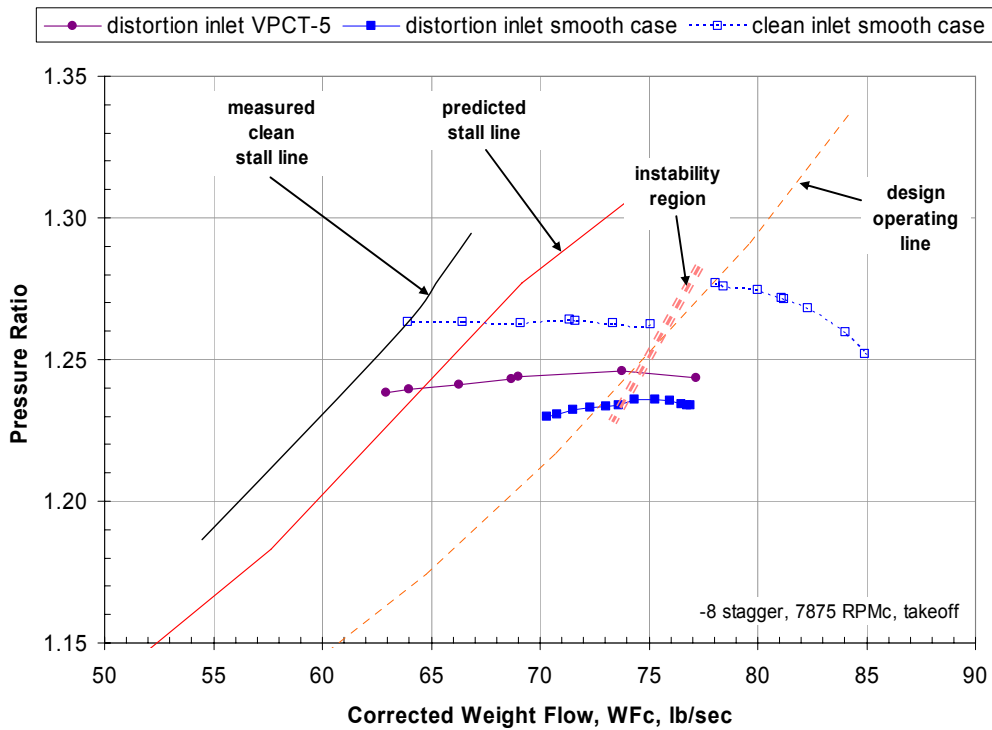
Figure 36.—Fan 2 pressure ratio versus corrected weight flow, with inlet distortion and VPCT–5.
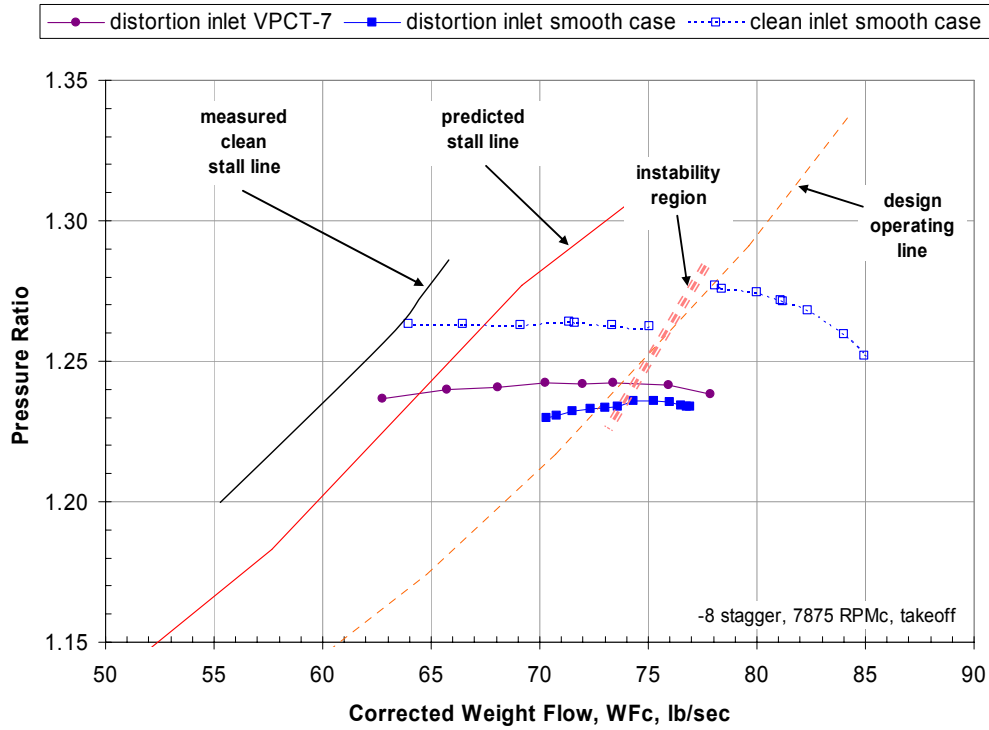
Figure 37.—Fan 2 pressure ratio versus corrected weight flow, with inlet distortion and VPCT–7.
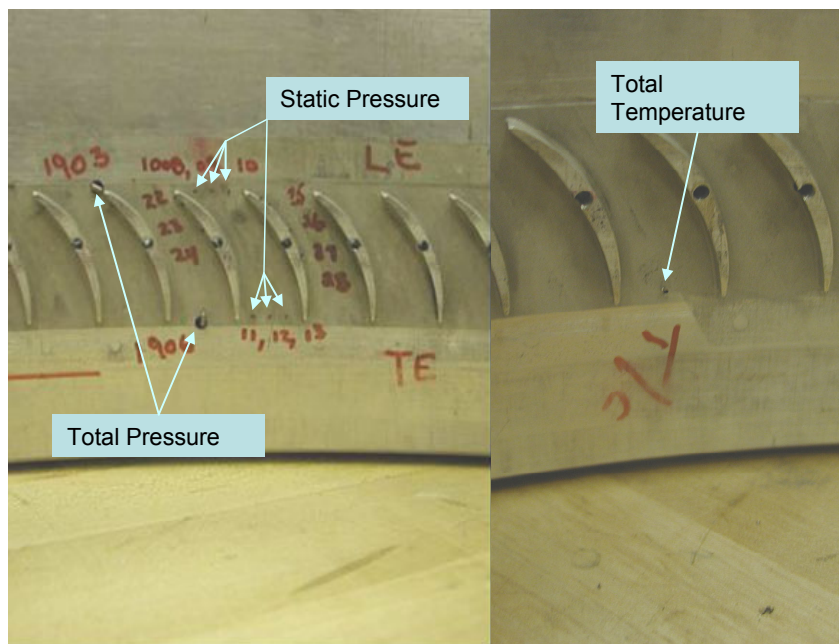
Figure 38.—VPCT internal instrumentation for pressures and temperature.
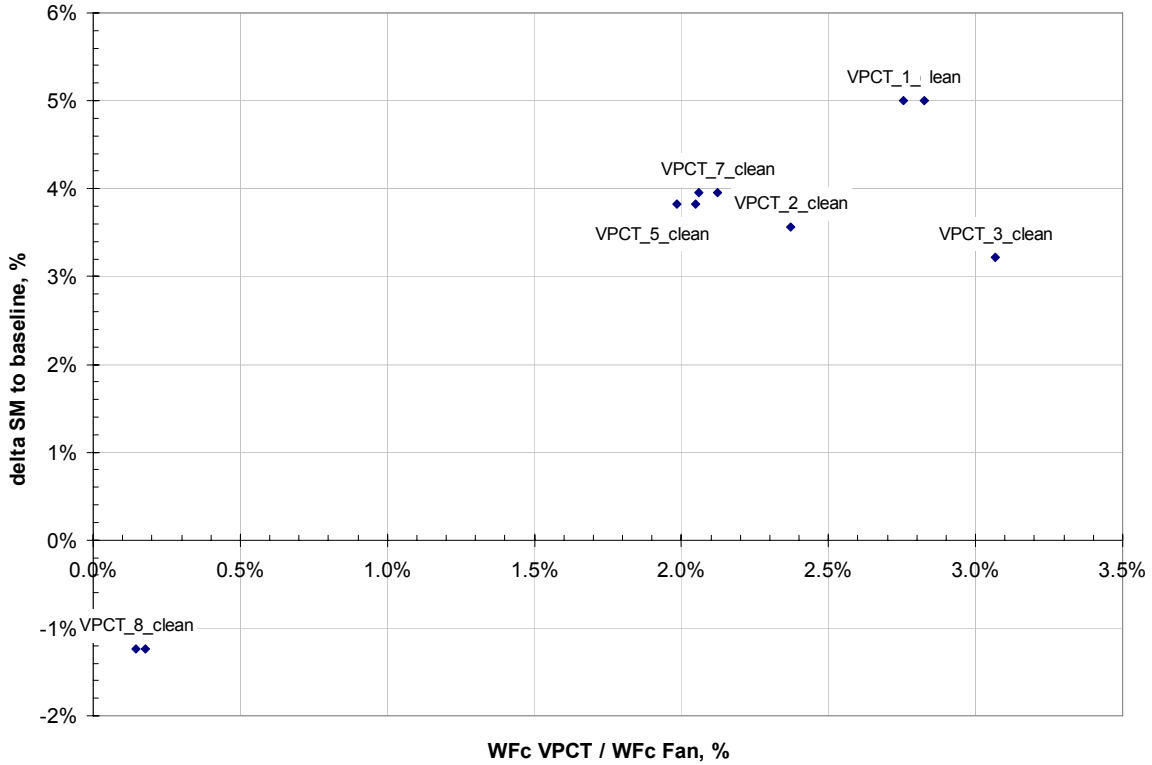
Figure 39.—Delta stall margin versus VPCT recirculation flow as percent of fan flow.
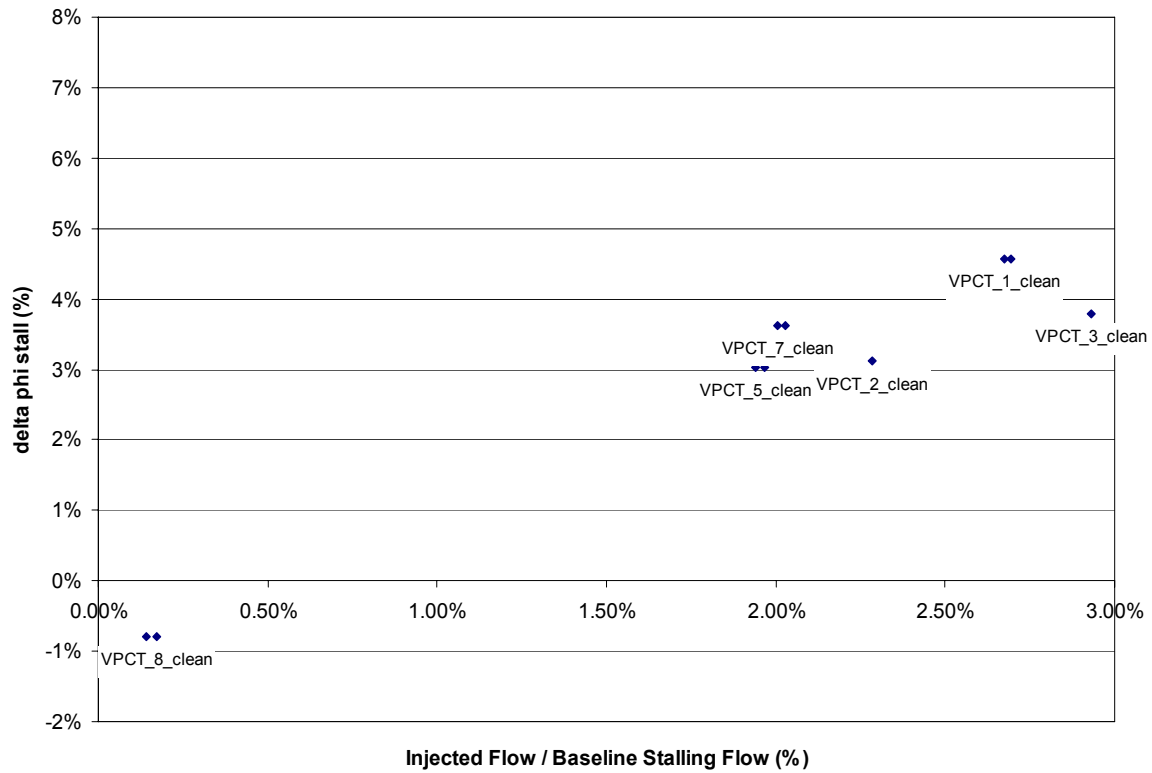
Figure 40.—Stalling flow coefficient versus percent of fan flow.
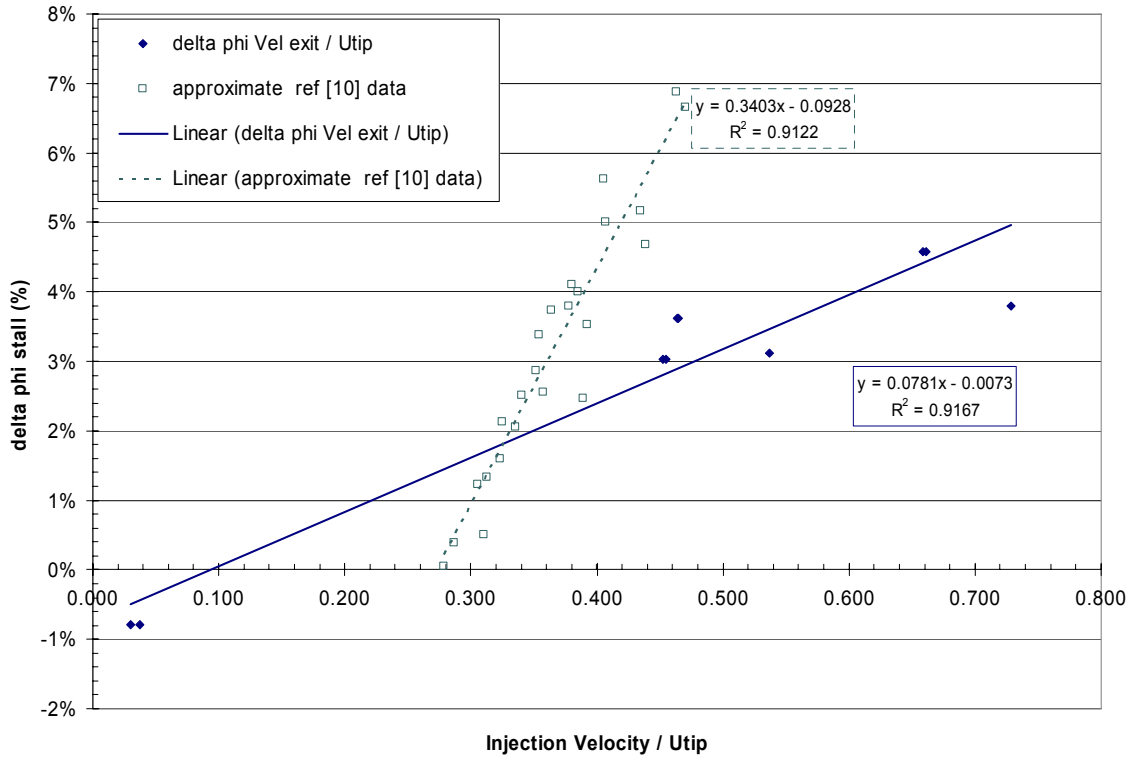
Figure 41.—Stalling flow coefficient comparison from (ref. 11).
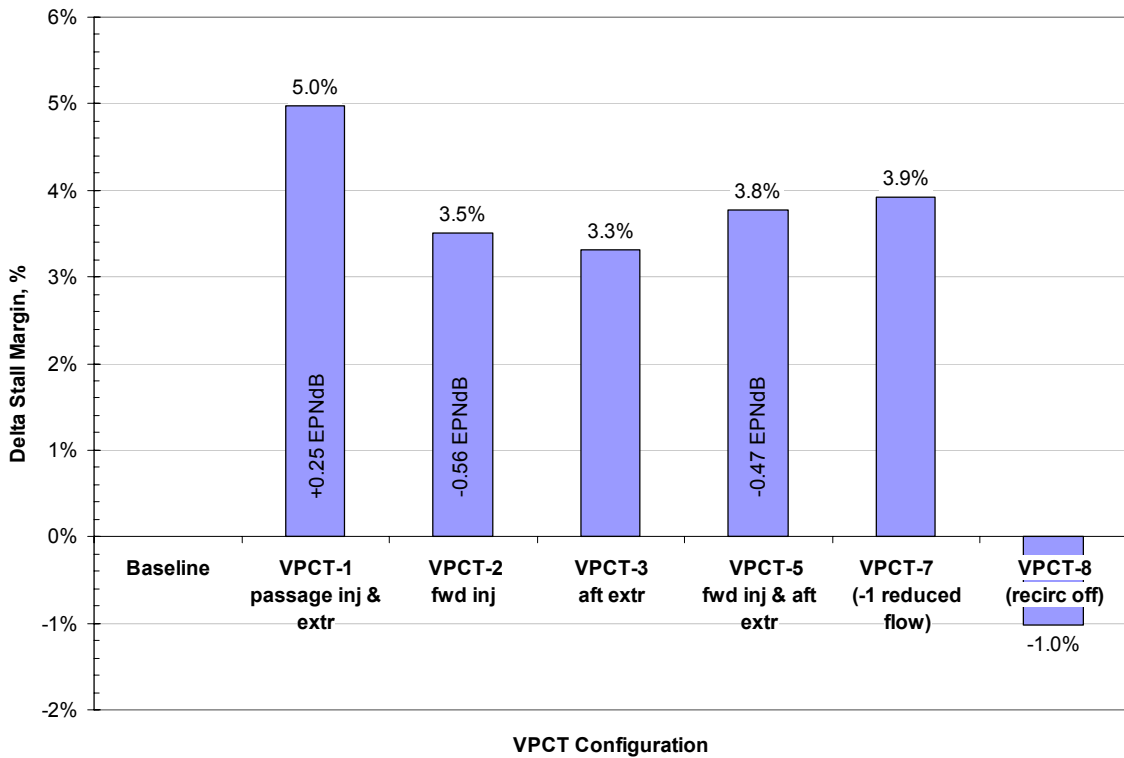
Figure 42.—VPCT Delta Stall Margin with clean inlet, no distortion.
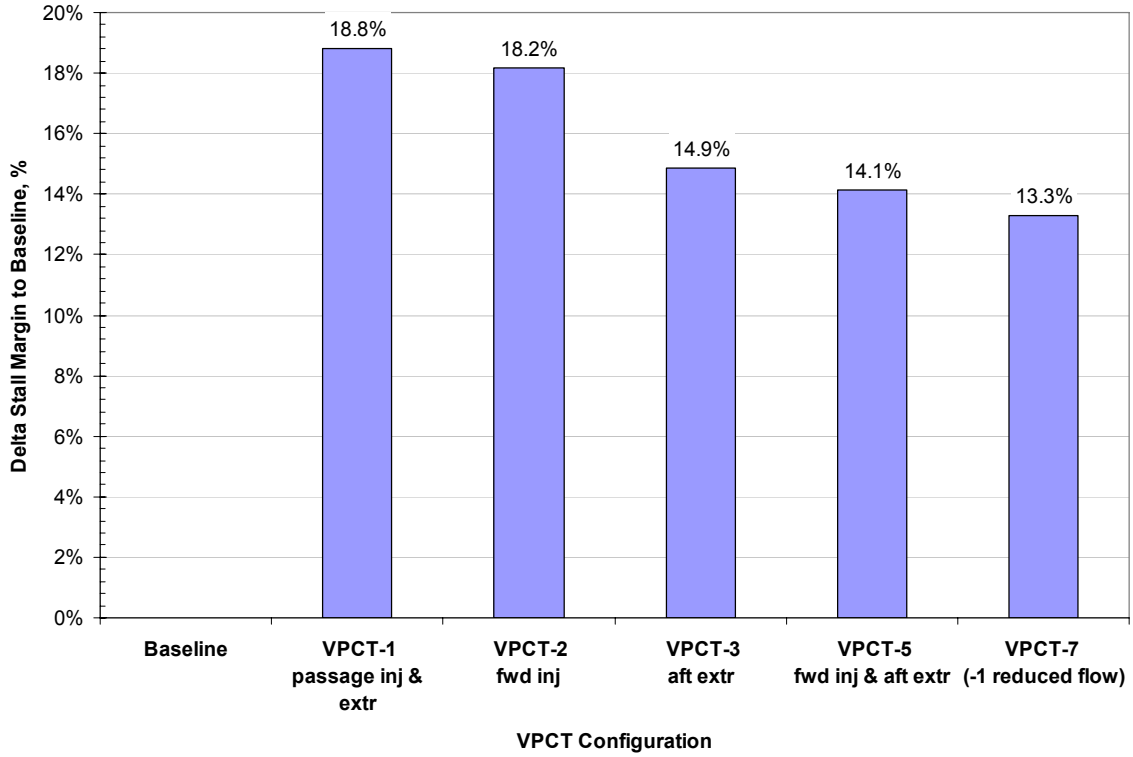
Figure 43.—VPCT Delta stall margin with inlet distortion.
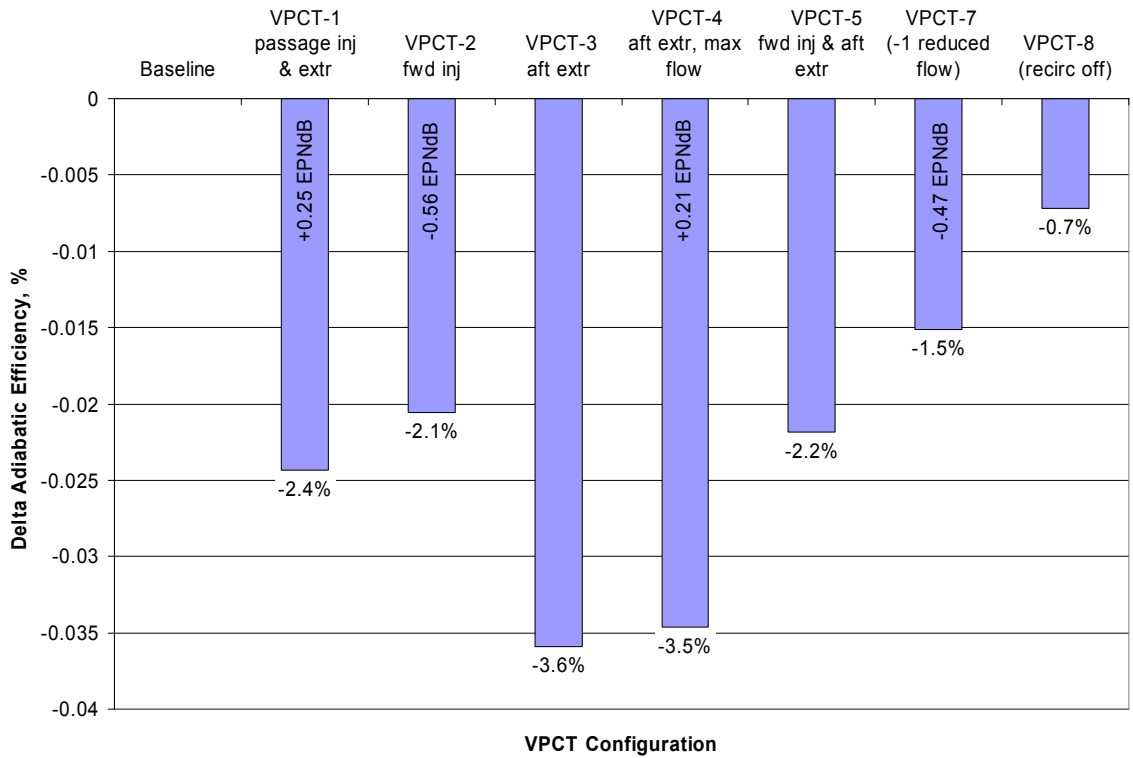
Figure 44.—VPCT Efficiency Comparisons with smooth inlet, no distortion.

Appendix A

Data for figure 9, baseline, 0° setting angle, smooth rubstrip

WFc	Fan Pressure Ratio
92.91	1.2952
92.66	1.2973
92.44	1.2992
92.37	1.2991
92.37	1.2994
91.89	1.3006
91.41	1.3020
90.93	1.3021
90.26	1.3002
90.00	1.2982
90.01	1.2983
89.96	1.2985
89.95	1.2984
89.89	1.2985
89.83	1.2986
89.83	1.2988
89.78	1.2985
89.78	1.2986
89.74	1.2986
89.75	1.2986
89.73	1.2983
89.70	1.2988
89.64	1.2984
89.64	1.2979
89.53	1.2982
89.51	1.2984
89.45	1.2980
89.43	1.2977
89.35	1.2974
89.33	1.2976
89.45	1.2972
89.31	1.2968
89.29	1.2966
89.22	1.2965
89.22	1.2961
89.15	1.2960
89.14	1.2955
89.13	1.2955
89.11	1.2954
89.04	1.2950
89.06	1.2952
89.05	1.2947

Data for figure 10, baseline, 0° setting angle, smooth rubstrip, radial profiles

Design Point (cruise) Profiles			Radius	PT12(n)	TT12(n)	AD EFF(n)
- Bypass		Bypass ID wall	5.810			
			6.204	1.1745	1.0523	0.9002
			6.924	1.2397	1.0664	0.9540
			7.577	1.2833	1.0743	0.9935
			8.177	1.3182	1.0827	0.9936
			8.737	1.3440	1.0881	1.0002
			9.263	1.3591	1.0919	0.9972
			9.760	1.3657	1.0941	0.9892
			10.233	1.3630	1.0969	0.9547
			10.685	1.3261	1.0989	0.8492
			11.119	1.3069	1.1104	0.7196
		Bypass OD wall	11.319			
Design Point (cruise) Profiles			Radius	PTCI(n)	TTCI(n)	AD EFF(n)
- Core		Core ID wall	4.491			
			4.601	1.0341	1.0325	0.2962
			4.758	1.0695	1.0371	0.5221
			4.916	1.1170	1.0445	0.7223
			5.073	1.1446	1.0478	0.8224
			5.231	1.1612	1.0476	0.9164
		Core OD wall	5.310			

Data for figures 11 and 12, Baseline, –8° stagger, smooth rubstrip, clean inlet

	WFc, lb/s	Fan Pressure Ratio	Fan Adiabatic Efficiency
4420	51.91	1.0712	0.8632
	51.84	1.0710	0.8446
	51.86	1.0711	0.8526
	51.42	1.0720	0.8686
	50.17	1.0739	0.8936
	49.41	1.0751	0.9046
	53.61	1.0769	0.9414
	51.64	1.0789	0.9518
	50.51	1.0798	0.9472
	50.68	1.0793	0.9422
	49.24	1.0801	0.9455
	46.80	1.0770	0.9444
	46.89	1.0768	0.9313
	45.99	1.0769	0.9326
	44.91	1.0768	0.9274
	43.84	1.0765	0.9318
	42.62	1.0766	0.9231
	41.57	1.0767	0.9170
	39.84	1.0775	0.9212
	39.17	1.0774	0.9194
	36.67	1.0781	0.9034
	35.24	1.0773	0.8376
5800	65.95	1.1387	0.9364
	64.48	1.1406	0.9365
	62.47	1.1423	0.9410
	60.93	1.1394	0.9783
6950	77.54	1.1988	0.9200
	75.98	1.2038	0.9304
	73.93	1.2077	0.9363
	72.89	1.2089	0.9375
	71.26	1.2087	0.9372
	71.32	1.2086	0.9353
	71.19	1.2084	0.9342
	68.99	1.2004	0.9292
	68.78	1.1998	0.9263
	66.89	1.1989	0.9205
	65.14	1.1993	0.9219
	63.38	1.2003	0.9226
	63.42	1.2003	0.9238
	61.60	1.2007	0.9193
	59.48	1.2005	0.9107
	57.08	1.2000	0.9029
	55.80	1.1999	0.8428

Data for figures 11 and 12, Baseline, –8° stagger, smooth rubstrip, clean inlet (continued)

	WFc, lb/s	Fan Pressure Ratio	Fan Adiabatic Efficiency
7450	82.04	1.2272	0.9046
	81.92	1.2273	0.9077
	80.58	1.2339	0.9231
	78.68	1.2388	0.9301
	76.18	1.2431	0.9350
	74.99	1.2440	0.9332
	67.33	1.2330	0.9199
	65.48	1.2331	0.9156
	62.98	1.2328	0.9096
	60.55	1.2323	0.8983
	60.35	1.2327	0.8988
7875	81.09	1.2718	0.9356
	84.94	1.2521	0.8981
	84.01	1.2598	0.9093
	82.32	1.2682	0.9249
	81.22	1.2715	0.9286
op pts	80.01	1.2746	0.9369
	78.41	1.2760	0.9360
	78.05	1.2771	0.9343
	75.08	1.2625	0.9183
	73.35	1.2628	0.9152
	71.60	1.2636	0.9179
	71.35	1.2640	0.9174
	69.09	1.2630	0.9116
	66.46	1.2632	0.9070
	63.93	1.2632	0.8559
8100	86.39	1.2592	0.8812
	85.56	1.2704	0.8960
	84.14	1.2807	0.9123
	83.10	1.2854	0.9218
	81.91	1.2884	0.9259
	80.51	1.2917	0.9276
	79.21	1.2935	0.9281

Data for figure 13 through 15, baseline, –8° stagger, smooth rubstrip, clean inlet

Takeoff Profiles, 7875 rpmc		Radius, in.	PT12(n)	TT12(n)	AD EFF(n)
Bypass	Duct ID	5.810			
		6.204	1.1612	1.0469	0.9309
		6.924	1.2144	1.0596	0.9574
		7.577	1.2549	1.0674	0.9951
		8.177	1.2900	1.0758	0.9958
		8.737	1.3158	1.0814	1.0022
		9.263	1.3328	1.0853	1.0027
		9.760	1.3425	1.0882	0.9954
		10.233	1.3439	1.0912	0.9659
		10.685	1.3270	1.0948	0.8883
		11.119	1.3254	1.1083	0.7739
	Duct OD	11.319			

Takeoff Profiles Core Inlet		Radius, in.	PTCI(n)	TTCI(n)	AD EFF(n)
	Duct ID	4.490			
		4.601	1.0613	1.0613	0.5921
		4.758	1.0798	1.0798	0.6591
		4.916	1.1172	1.1172	0.8035
		5.073	1.1302	1.1302	0.8799
		5.231	1.1394	1.1394	0.9223
	Duct OD	5.310			

Cutback Profiles, 6950 rpmc		Radius, in.	PT121(n)	TT12(n)	Eff12(n)
Bypass	Duct ID	5.810			
		6.204	1.1275	1.0377	0.9246
		6.924	1.1667	1.0463	0.9721
		7.577	1.1958	1.0526	0.9974
		8.177	1.2207	1.0589	0.9946
		8.737	1.2392	1.0637	0.9926
		9.263	1.2523	1.0665	0.9982
		9.760	1.2578	1.0685	0.9891
		10.233	1.2591	1.0698	0.9746
		10.685	1.2466	1.0726	0.8953
		11.119	1.2334	1.0815	0.7576
	Duct OD	11.319			

Cutback Profiles Core		Radius, in.	PTCI(n)	TTCI(n)	EffCI(n)
	Duct ID	4.490			
		4.601	1.0521	1.0243	0.6009
		4.758	1.0636	1.0268	0.6630
		4.916	1.0913	1.0322	0.7848
		5.073	1.1010	1.0324	0.8594
		5.231	1.1086	1.0335	0.8933
	Duct OD	5.310			

Data for figure 13 through 15, baseline, –8° stagger, smooth rubstrip, clean inlet (continued)

Approach Profiles, 4420 rpmc		Radius, in.	PT121(n)	TT12(n)	AD EFF(n)
Bypass	Duct ID	5.810			
		6.204	1.0499	1.0148	0.9446
		6.924	1.0648	1.0181	0.9986
		7.577	1.0757	1.0209	1.0081
		8.177	1.0856	1.0240	0.9914
		8.737	1.0921	1.0252	1.0114
		9.263	1.0967	1.0262	1.0188
		9.760	1.0987	1.0270	1.0099
		10.233	1.0999	1.0273	1.0106
		10.685	1.0950	1.0281	0.9344
		11.119	1.0850	1.0307	0.7670
	Duct OD	11.319			
Approach Profiles					
Core		Radius, in.	PTCI(n)	TTCI(n)	AD EFFI(n)
	Duct ID	4.490			
		4.601	1.0171	1.0111	0.4374
		4.758	1.0218	1.0114	0.5433
		4.916	1.0322	1.0134	0.6777
		5.073	1.0383	1.0135	0.7968
		5.231	1.0410	1.0141	0.8156
	Duct OD	5.310			

Data for figure 16
TIP CLEARANCE, mils

		pwtip1	pwtip2	pwtip3	pwtip4	pwtip5	pwtip6	pwtip7	pwtip8
ESCORT									
rdg	rpm	LE, 45	LE, 135	LE, 225	LE, 315	TE, 45	TE, 135	TE, 225	TE, 315
2303	2014.5	48.2	45.7	54.8	59.5	49.0	48.8	49.8	55.7
2304	2022.0	48.2	45.6	55.0	59.8	49.2	48.9	49.8	55.9
2305	177.0	49.9	47.3	56.2	61.6	51.8	50.8	51.9	58.6
2306	4477.9	44.3	44.4	52.4	57.1	46.1	46.2	47.1	52.9
2307	4476.8	44.5	44.7	52.2	57.4	46.2	46.4	46.9	52.9
2308	4477.5	44.6	45.0	52.6	57.5	46.5	46.9	47.2	53.3
2309	4474.9	44.7	45.1	52.8	57.8	46.5	46.9	47.3	53.4
2310	4476.0	44.7	45.1	52.9	57.8	46.6	46.9	47.4	53.4
2311	4475.6	44.7	45.4	53.1	57.9	46.8	47.2	47.5	53.5
2312	4474.1	44.8	45.5	53.5	58.4	46.8	47.1	47.5	53.5
2313	4475.2	44.7	45.3	53.2	58.0	46.8	47.2	47.6	53.5
2314	4476.0	44.7	45.3	53.3	57.9	46.7	47.2	47.7	53.5
2315	6069.4	42.5	43.7	50.5	55.5	42.8	43.6	44.5	49.7
2316	6067.9	42.7	44.1	51.3	56.1	43.4	44.1	45.3	50.3
2317	7968.8	39.7	42.5	50.1	54.2	37.5	40.2	41.4	46.5
2318	7975.9	40.1	43.6	51.6	55.0	37.5	40.7	41.9	46.7
2319	7964.6	40.2	43.5	51.5	54.9	37.7	40.8	41.9	46.6
2320	7968.0	40.2	43.6	51.3	54.9	37.9	41.1	42.0	46.9
2321	7976.3	40.3	43.5	51.2	55.0	38.0	40.9	41.8	47.0
2322	7969.1	40.1	43.4	51.3	55.3	38.1	41.1	42.2	47.5
2323	7974.8	40.4	43.3	51.3	55.3	38.0	41.2	42.3	47.5
2324	7944.0	40.4	43.5	51.4	55.2	38.1	41.0	41.9	47.0
2325	7962.8	40.4	43.5	50.7	54.8	38.3	41.2	41.7	46.9
2326	7959.4	40.5	43.4	51.1	54.9	38.2	41.2	42.0	47.2
2327	7966.9	40.4	43.4	51.2	54.9	38.2	41.2	42.0	47.2
2328	7537.5	41.1	43.5	51.6	55.3	38.8	42.4	42.1	48.5
2329	7533.4	39.6	41.6	49.2	53.1	37.5	40.9	40.5	46.7
2330	7527.8	40.9	43.0	50.7	54.5	38.9	42.4	42.0	48.3
2331	7527.8	40.7	43.0	50.7	54.6	39.1	42.7	42.2	48.5
2332	7530.8	41.0	43.0	50.7	54.9	39.4	42.7	42.2	49.0
2333	7531.1	41.4	43.3	51.1	55.4	39.9	42.9	42.5	49.3
2334	7028.3	41.5	43.4	52.1	55.6	41.2	42.9	43.8	49.2
2335	7026.8	41.4	43.2	51.8	55.4	41.3	42.9	43.9	49.0
2336	7024.1	41.4	43.1	51.7	55.4	41.4	42.9	44.1	49.0
2337	7024.5	41.2	43.1	51.7	55.4	41.5	42.8	44.3	49.2
2338	7030.1	41.4	43.2	51.7	55.5	41.4	43.1	44.3	49.2
2339	7027.5	41.7	43.0	51.8	55.5	41.1	43.3	43.7	49.9
2340	7038.0	41.6	42.9	52.0	55.5	40.9	43.6	43.5	49.9
2341	5866.9	42.5	44.1	52.6	57.3	44.3	45.3	46.9	52.4
2342	5872.9	42.4	44.1	52.4	57.0	44.1	45.2	46.7	52.0
2343	5872.9	41.9	44.0	52.3	56.9	44.1	45.1	46.6	52.0
2344	5865.8	42.4	44.0	52.3	56.9	44.1	45.1	46.6	52.0
2345	4475.6	43.5	45.1	54.1	58.8	47.4	48.3	49.3	55.3
2346	4476.0	43.7	44.9	53.9	58.5	47.3	48.0	49.0	55.1

Data for figure 16 (continued)

<u>TIP CLEARANCE, mils</u>

		pwtip1	pwtip2	pwtip3	pwtip4	pwtip5	pwtip6	pwtip7	pwtip8
ESCORT									
rdg	rpm	LE, 45	LE, 135	LE, 225	LE, 315	TE, 45	TE, 135	TE, 225	TE, 315
2347	4468.9	43.7	44.9	54.0	58.8	47.3	48.0	48.9	55.0
2348	4470.0	43.4	44.6	53.7	58.3	47.1	47.7	48.7	54.8
2349	4477.1	43.9	44.6	53.6	58.4	47.1	47.7	48.7	54.8
2350	4474.9	43.4	44.5	53.6	58.3	46.9	47.6	48.5	54.7
2351	4469.6	43.2	44.6	53.6	58.1	47.1	47.6	48.6	54.8
2352	4471.1	43.7	44.5	53.6	58.3	46.9	47.4	48.5	54.8
2353	4469.2	43.5	44.6	53.6	58.1	46.9	47.6	48.5	54.6
2354	4470.8	43.6	44.6	53.6	58.3	46.9	47.4	48.6	54.7
2355	4468.1	43.6	44.7	53.7	58.4	46.9	47.4	48.7	54.7
2356	4476.0	43.7	44.8	53.6	58.5	46.9	47.5	48.5	54.9
2357	4472.2	43.7	44.7	53.7	58.5	47.0	47.5	48.7	54.9
2358	4467.8	44.0	44.9	53.6	58.4	47.0	47.4	48.4	54.8
2359	4471.9	44.0	44.7	53.6	58.4	47.1	47.6	48.5	54.8
2360	8192.2	39.0	42.6	50.1	53.0	35.8	39.2	40.0	44.3
2361	8194.9	39.1	42.9	50.6	53.2	36.4	39.8	40.6	44.9
2362	8202.8	39.4	43.2	50.9	53.6	36.9	40.2	41.1	45.1
2363	8193.4	39.7	43.2	51.1	54.1	37.4	40.5	41.2	45.5
2364	8191.9	39.8	43.2	51.3	54.3	37.9	40.7	41.5	45.9
2365	8199.8	39.7	43.2	51.3	54.4	37.9	40.8	41.7	46.0
2366	8193.8	39.7	43.2	51.6	54.5	37.9	40.7	42.0	46.3
2367	8761.5	39.6	43.1	50.1	53.4	35.3	39.0	38.5	43.8
2368	4473.4	43.6	45.0	54.1	58.4	47.1	47.8	48.7	54.5

Data for figure 17		
RPMc	**WFc**	**Overall PR**
4420	51.24	1.0699
	50.15	1.0717
	49.35	1.0729
	47.71	1.0738
	52.74	1.0763
	51.62	1.0768
	50.45	1.0777
	49.12	1.0787
	49.06	1.0787
	46.84	1.0762
	45.87	1.0756
	44.78	1.0757
	43.82	1.0757
	42.83	1.0759
	41.58	1.0762
	40.60	1.0765
	39.43	1.0769
	38.22	1.0772
	37.02	1.0774
	35.53	1.0774
	33.46	1.0740
	33.28	1.0737
	32.49	1.0722
	29.31	1.0583
	27.34	1.0487
	26.94	1.0486
	26.56	1.0482
	26.74	1.0482
5800	64.54	1.1366
	63.85	1.1374
	62.09	1.1391
	60.82	1.1387
	59.05	1.1343
	57.46	1.1334
	56.12	1.1340
	54.67	1.1342
	53.10	1.1346
	51.71	1.1348
	50.10	1.1354
	48.44	1.1357
	46.52	1.1361
	44.74	1.1346
6950	76.04	1.1952
	76.08	1.1952
	75.18	1.1977
	73.37	1.2013
	73.35	1.2012
	72.34	1.2028
	71.11	1.2040
	70.07	1.2030

Data for figure 17 (continued)		
RPMc	**WFc**	**Overall PR**
7450	80.25	1.2202
	79.48	1.2245
	77.82	1.2306
	75.65	1.2347
	74.23	1.2364
	73.31	1.2350
	71.57	1.2298
	71.34	1.2287
	69.31	1.2291
	67.59	1.2298
	65.56	1.2298
	63.46	1.2308
	61.02	1.2313
	58.94	1.2301
	57.59	1.2296
7875	83.39	1.2404
	83.36	1.2404
	82.60	1.2476
	81.19	1.2561
	81.16	1.2560
	80.16	1.2595
op pts	79.04	1.2627
	77.61	1.2659
	76.58	1.2663
	74.49	1.2600
	72.98	1.2587
	70.90	1.2598
	69.17	1.2605
	66.74	1.2613
	64.50	1.2621
	61.99	1.2586
	61.01	1.2576
8100	84.68	1.2490
	84.00	1.2575
	82.76	1.2678
	81.95	1.2724
	80.88	1.2763
	79.62	1.2801
	77.90	1.2816
	77.87	1.2815
	77.54	1.2815
	75.69	1.2750
	74.78	1.2746
	72.70	1.2751
	70.99	1.2766
	68.45	1.2779
	66.17	1.2782
	63.35	1.2740
	62.84	1.2728

Data for figure 18

7875 VPCT-1				7875 Baseline		
RPMc	**WFc**	**Overall PR**		**RPMc**	**WFc**	**Overall PR**
7875	83.39	1.2404		7875	81.09	1.2718
	83.36	1.2404			84.94	1.2521
	82.60	1.2476			84.01	1.2598
	81.19	1.2561			82.32	1.2682
	81.16	1.2560			81.22	1.2715
	80.16	1.2595	op pts	80.01	1.2746
op pts	79.04	1.2627			78.41	1.2760
	77.61	1.2659			78.05	1.2771
	76.58	1.2663			75.08	1.2625
	74.49	1.2600			73.35	1.2628
	72.98	1.2587			71.60	1.2636
	70.90	1.2598			71.35	1.2640
	69.17	1.2605			69.09	1.2630
	66.74	1.2613			66.46	1.2632
	64.50	1.2621			63.93	1.2632
	61.99	1.2586				
	61.01	1.2576				

Data for figure 19(a)

Radius	TO PT Ratio	CB PT Ratio	APP PT Ratio
11.319	Bypass OD wall		
11.119	1.2845	1.2192	1.0816
10.685	1.2986	1.2380	1.0931
10.233	1.3306	1.2522	1.0967
9.760	1.3323	1.2516	1.0964
9.263	1.3246	1.2460	1.0950
8.737	1.3100	1.2347	1.0909
8.177	1.2856	1.2168	1.0845
7.577	1.2518	1.1930	1.0751
6.924	1.2116	1.1653	1.0643
6.204	1.1603	1.1269	1.0491
5.810	Bypass ID wall		
5.310	Core OD wall		
5.231	1.1385	1.1084	1.0409
5.073	1.1273	1.0999	1.0380
4.916	1.1154	1.0916	1.0316
4.758	1.0800	1.0638	1.0216
4.601	1.0611	1.0534	1.0168
4.490	Core ID wall		

Data for figure 19(b)

Radius	TO TT Ratio	CB TT Ratio	APP TT Ratio
11.319	Bypass OD wall		
11.119	1.1204	1.0911	1.0334
10.685	1.0955	1.0722	1.0270
10.233	1.0886	1.0676	1.0264
9.760	1.0860	1.0672	1.0265
9.263	1.0839	1.0652	1.0258
8.737	1.0804	1.0625	1.0247
8.177	1.0751	1.0581	1.0232
7.577	1.0665	1.0518	1.0204
6.924	1.0589	1.0457	1.0176
6.204	1.0471	1.0374	1.0144
5.810	Bypass ID wall		
5.310	Core OD wall		
5.231	1.0414	1.0330	1.0130
5.073	1.0398	1.0315	1.0129
4.916	1.0386	1.0315	1.0123
4.758	1.0327	1.0264	1.0105
4.601	1.0284	1.0231	1.0102
4.490	Core ID wall		

Data for figure 19(c)

Radius	TO EFF	CB EFF	APP EFF
11.319	Bypass OD wall		
11.119	0.6158	0.6393	0.6787
10.685	0.8113	0.8711	0.9549
10.233	0.9601	0.9816	1.0119
9.760	0.9936	0.9858	1.0059
9.263	0.9971	0.9956	1.0186
8.737	0.9977	0.9933	1.0198
8.177	0.9913	0.9921	1.0100
7.577	0.9964	0.9986	1.0236
6.924	0.9579	0.9768	1.0235
6.204	0.9218	0.9272	0.9567
5.810	Bypass ID wall		
5.310	Core OD wall		
5.231	0.9127	0.9034	0.8900
5.073	0.8747	0.8757	0.8277
4.916	0.8202	0.8039	0.7241
4.758	0.6802	0.6764	0.5822
4.601	0.6004	0.6495	0.4686
4.490	Core ID wall		

Data for figure 20

7875 VPCT–2

WFc	Overall PR
83.07	1.2521
81.69	1.2611
81.60	1.2612
80.73	1.2649
79.57	1.2684
79.00	1.2699
78.48	1.2705
77.79	1.2712
76.84	1.2703
76.81	1.2699
71.18	1.2631
72.63	1.2631
73.40	1.2633
68.99	1.2638
66.62	1.2641
64.34	1.2642
62.96	1.2621
61.94	1.2613

Data for figure 21

7875 VPCT–3

WFc	Overall PR
83.43	1.2391
82.50	1.2469
81.03	1.2546
80.03	1.2578
78.85	1.2615
78.32	1.2631
77.80	1.2641
77.08	1.2650
71.16	1.2599
71.16	1.2600
72.51	1.2589
73.29	1.2588
68.85	1.2610
66.42	1.2620
64.09	1.2630
62.68	1.2611
61.51	1.2595

Data for figure 22

7875 VPCT–4

WFc	Overall PR
83.09	1.2377
82.18	1.2451
80.79	1.2532
79.85	1.2570
79.18	1.2591
78.64	1.2609
78.13	1.2616

Data for figure 23

7875 VPCT–5

WFc	Overall PR
84.00	1.2447
83.19	1.2531
81.85	1.2620
80.90	1.2656
79.62	1.2692
78.30	1.2718
76.84	1.2714
71.75	1.2637
73.16	1.2636
69.35	1.2638
66.97	1.2641
64.65	1.2646
64.63	1.2646
62.29	1.2617
62.00	1.2619

Data for figure 24

7875 VPCT–7

WFc	Overall PR
82.93	1.2532
81.41	1.2612
80.45	1.2641
79.26	1.2675
77.78	1.2698
76.81	1.2689
70.79	1.2612
68.69	1.2624
66.20	1.2632
63.65	1.2629
61.62	1.2606

Data for figure 25

7875 VPCT–8

WFc	Overall PR
84.71	1.2494
83.74	1.2574
82.08	1.2659
81.05	1.2690
79.70	1.2718
78.06	1.2728
73.73	1.2608
72.90	1.2604
71.12	1.2616
68.88	1.2620
66.29	1.2624
64.44	1.2629

Data for figure 26(a) and (b)

Radius	baseline PT ratio	VPCT–1 PT ratio	VPCT–2 PT ratio	VPCT–3 PT ratio	VPCT–4 PT ratio	VPCT–5 PT ratio	VPCT–7 PT ratio	VPCT–8 PT ratio
5.810	Bypass Duct ID							
6.204	1.1612	1.1603	1.1611	1.1614	1.1618	1.1613	1.1610	1.1607
6.924	1.2144	1.2116	1.2123	1.2117	1.2132	1.2127	1.2124	1.2129
7.577	1.2549	1.2518	1.2537	1.2525	1.2526	1.2531	1.2535	1.2545
8.177	1.2900	1.2856	1.2877	1.2860	1.2869	1.2879	1.2876	1.2898
8.737	1.3158	1.3100	1.3131	1.3105	1.3107	1.3132	1.3128	1.3156
9.263	1.3328	1.3246	1.3285	1.3250	1.3248	1.3291	1.3280	1.3316
9.760	1.3425	1.3323	1.3384	1.3323	1.3310	1.3387	1.3366	1.3417
10.233	1.3439	1.3306	1.3406	1.3263	1.3236	1.3413	1.3364	1.3403
10.685	1.3270	1.2986	1.3199	1.2910	1.2806	1.3164	1.3100	1.3163
11.119	1.3254	1.2845	1.3017	1.2918	1.2763	1.3010	1.2979	1.3122
11.319	Bypass Duct OD							

Data for figure 27(a) and (b)

Radius	baseline TT ratio	VPCT–1 TT ratio	VPCT–2 TT ratio	VPCT–3 TT ratio	VPCT–4 TT ratio	VPCT–5 TT ratio	VPCT–7 TT ratio	VPCT–8 TT ratio
5.810	Bypass Duct ID							
6.204	1.0469	1.0471	1.0474	1.0474	1.0472	1.0474	1.0469	1.0469
6.924	1.0596	1.0589	1.0599	1.0593	1.0590	1.0593	1.0592	1.0595
7.577	1.0674	1.0665	1.0674	1.0670	1.0668	1.0670	1.0669	1.0673
8.177	1.0758	1.0751	1.0758	1.0752	1.0750	1.0756	1.0753	1.0757
8.737	1.0814	1.0804	1.0816	1.0808	1.0803	1.0813	1.0809	1.0816
9.263	1.0853	1.0839	1.0854	1.0845	1.0836	1.0853	1.0848	1.0855
9.760	1.0882	1.0860	1.0881	1.0867	1.0857	1.0879	1.0871	1.0882
10.233	1.0912	1.0886	1.0906	1.0917	1.0916	1.0908	1.0898	1.0917
10.685	1.0948	1.0955	1.0970	1.0994	1.0991	1.0995	1.0958	1.0959
11.119	1.1083	1.1204	1.1186	1.1250	1.1262	1.1215	1.1180	1.1090
11.319	Bypass Duct OD							

Data for figure 28(a) and (b)

Radius	baseline Ad. Eff.	VPCT–1 Ad. Eff.	VPCT–2 Ad. Eff.	VPCT–3 Ad. Eff.	VPCT–4 Ad. Eff.	VPCT–5 Ad. Eff.	VPCT–7 Ad. Eff.	VPCT–8 Ad. Eff.
5.810	Bypass Duct ID							
6.204	0.9309	0.9218	0.9192	0.9217	0.9269	0.9214	0.9290	0.9269
6.924	0.9574	0.9579	0.9433	0.9517	0.9616	0.9553	0.9551	0.9533
7.577	0.9951	0.9964	0.9897	0.9912	0.9948	0.9932	0.9961	0.9941
8.177	0.9958	0.9913	0.9889	0.9915	0.9964	0.9911	0.9949	0.9959
8.737	1.0022	0.9977	0.9921	0.9935	1.0009	0.9962	0.9992	0.9989
9.263	1.0027	0.9971	0.9901	0.9914	1.0009	0.9926	0.9955	0.9969
9.760	0.9954	0.9936	0.9854	0.9854	0.9939	0.9890	0.9926	0.9932
10.233	0.9659	0.9601	0.9648	0.9166	0.9110	0.9638	0.9618	0.9522
10.685	0.8883	0.8113	0.8513	0.7614	0.7386	0.8210	0.8369	0.8520
11.119	0.7739	0.6158	0.6595	0.6070	0.5722	0.6425	0.6553	0.7409
11.319	Bypass Duct OD							

Data for figure 30

Radius	Pole Rake 12° PT20	Pole Rake 160° PT20	Pole Rake 180° PT20	Pole Rake 220° PT20
5.464	1.0002	1.0002	1.0001	1.0001
6.186	1.0001	1.0001	1.0002	0.9999
6.908	1.0000	1.0002	1.0001	0.9999
7.63	1.0001	1.0002	1.0001	1.0000
7.99	1.0003	1.0001	1.0001	1.0001
8.351	1.0001	1.0001	1.0001	1.0001
8.712	1.0001	1.0001	1.0000	1.0002
9.073	1.0002	0.9969	0.9913	0.9962
9.434	1.0002	0.8934	0.8777	0.9030
9.794	1.0002	0.8426	0.8306	0.8406
10.155	0.9994	0.8146	0.8100	0.8301
10.518	flowpath wall			

Data for figure 31

Radius	BL 140° BL20	BL 200° BL20	BL 270° BL20	BL 348° BL20
8.929	0.9995	0.9995	1.0002	1.0000
9.217	0.9400	0.9468	1.0000	1.0001
9.578	0.8397	0.8441	1.0001	1.0000
9.794	0.8216	0.8249	0.9996	1.0001
10.083	0.8025	0.8131	0.9996	1.0000
10.191	0.7954	0.8095	0.9967	0.9984
10.300	0.7925	0.8056	0.9870	0.9897
10.372	0.7905	0.8029	0.9752	0.9784
10.444	0.7894	0.7990	0.9313	0.9321
10.518	flowpath wall			

Data for figure 32

7875 distortion inlet

WFc	Overall PR
76.93	1.2340
76.77	1.2338
76.50	1.2343
75.97	1.2354
75.27	1.2360
74.33	1.2361
73.62	1.2339
73.02	1.2333
72.32	1.2330
71.51	1.2322
70.78	1.2308
70.31	1.2298

7875 clean inlet

WFc	Overall PR
63.93	1.2632
66.46	1.2632
69.09	1.2630
71.35	1.2640
71.60	1.2636
73.35	1.2628
75.08	1.2625
78.05	1.2771
78.41	1.2760
80.01	1.2746
81.09	1.2718
81.22	1.2715
82.32	1.2682
84.01	1.2598
84.94	1.2521

Data for figure 33

7875 VPCT–1 distortion

WFC	Overall PR
78.78	1.2347
78.38	1.2363
77.68	1.2381
76.83	1.2403
75.90	1.2418
74.77	1.2436
73.48	1.2440
72.22	1.2441
71.39	1.2445
70.65	1.2439
68.67	1.2422
66.61	1.2423
64.32	1.2425
62.15	1.2413
60.61	1.2395

Data for figure 34

7875 VPCT–2 distortion

WFC	Overall PR
78.95	1.2371
78.22	1.2399
76.35	1.2480
73.97	1.2515
72.41	1.2511
70.85	1.2503
69.16	1.2483
66.78	1.2454
64.62	1.2434
61.60	1.2419

Data for figure 35

7875 VPCT–3 distortion

WFC	Overall PR
76.45	1.2457
73.12	1.2513
68.42	1.2484
65.91	1.2457
63.56	1.2433
61.97	1.2420

Data for figure 36

7875 VPCT–5 distortion

WFC	Overall PR
77.15	1.2435
73.79	1.2460
69.02	1.2439
68.67	1.2430
66.28	1.2412
63.96	1.2397
62.93	1.2381

Data for figure 37

7875 VPCT–7 distortion

WFC	Overall PR
77.87	1.2382
75.95	1.2415
73.37	1.2424
71.97	1.2421
70.25	1.2421
68.10	1.2408
65.73	1.2398
62.74	1.2365

	Data for figure 39			**Data for figure 40**		
	WFc vpct / WFc fan, (%)	**ΔSM rel to baseline smooth case (%)**		**Inj flow/ baseline stalling flow, (%)**	**Δ Phi stall, (%)**
VPCT 1 clean	2.75	5.00	**VPCT 1 clean**	2.67	4.57
VPCT 1 clean	2.83	5.00	**VPCT 1 clean**	2.69	4.57
VPCT 2 clean	2.37	3.57	**VPCT 2 clean**	2.28	3.12
VPCT 3 clean	3.07	3.22	**VPCT 3 clean**	2.93	3.80
VPCT 5 clean	1.99	3.82	**VPCT 5 clean**	1.94	3.02
VPCT 5 clean	2.05	3.82	**VPCT 5 clean**	1.97	3.02
VPCT 7 clean	2.06	3.95	**VPCT 7 clean**	2.00	3.62
VPCT 7 clean	2.12	3.95	**VPCT 7 clean**	2.03	3.62
VPCT 8 clean	0.18	−1.24	**VPCT 8 clean**	0.17	−0.80
VPCT 8 clean	0.15	−1.24	**VPCT 8 clean**	0.14	−0.80

REPORT DOCUMENTATION PAGE

Public reporting burden for this collection of information is estimated to average 1 hour per response, including the time for reviewing instructions, searching existing data sources, gathering and maintaining the data needed, and completing and reviewing the collection of information. Send comments regarding this burden estimate or any other aspect of this collection of information, including suggestions for reducing this burden, to Washington Headquarters Services, Directorate for Information Operations and Reports, 1215 Jefferson Davis Highway, Suite 1204, Arlington, VA 22202-4302, and to the Office of Management and Budget, Paperwork Reduction Project (0704-0188), Washington, DC 20503.

1. AGENCY USE ONLY (Leave blank)	2. REPORT DATE April 2006	3. REPORT TYPE AND DATES COVERED Technical Memorandum

4. TITLE AND SUBTITLE

Fan Performance From Duct Rake Instrumentation on a 1.294 Pressure Ratio, 725 ft/sec Tip Speed Turbofan Simulator Using Vaned Passage Casing Treatment

5. FUNDING NUMBERS

WBS 561581.02.08.03.03.01

6. AUTHOR(S)

E. Brian Fite

7. PERFORMING ORGANIZATION NAME(S) AND ADDRESS(ES)

National Aeronautics and Space Administration
John H. Glenn Research Center at Lewis Field
Cleveland, Ohio 44135–3191

8. PERFORMING ORGANIZATION REPORT NUMBER

E–15487

9. SPONSORING/MONITORING AGENCY NAME(S) AND ADDRESS(ES)

National Aeronautics and Space Administration
Washington, DC 20546–0001

10. SPONSORING/MONITORING AGENCY REPORT NUMBER

NASA TM—2006-214241

11. SUPPLEMENTARY NOTES

Responsible person, E. Brian Fite, organization code RTA, 216–433–3892.

12a. DISTRIBUTION/AVAILABILITY STATEMENT

Unclassified - Unlimited
Subject Category: 02

Available electronically at http://gltrs.grc.nasa.gov

This publication is available from the NASA Center for AeroSpace Information, 301–621–0390.

12b. DISTRIBUTION CODE

13. ABSTRACT (Maximum 200 words)

A 1.294 pressure ratio, 725 ft/sec tip speed, variable pitch low noise fan was designed and tested in the NASA Glenn 9-by 15-foot Wind Tunnel. The design included a casing treatment that used recirculation to extend the fan stall line and provide an acceptable operating range. Overall aerodynamic experimental results are presented for this low tip speed, low noise fan without casing treatment as well as using several variants of the casing treatment that moved the air extraction and insertion axial locations. Measurements were made to assess effects on performance, operability, and noise. An unusual instability was discovered near the design operating line and is documented in the fan operating range. Measurements were made to compare stall margin improvements as well as measure the performance impact of the casing treatments. Experimental results in the presence of simulated inlet distortion, via screens, are presented for the baseline and recirculation casing treatment configurations. Estimates are made for the quantity of recirculation weight flow based on limited instrumentation in the recirculation system along with discussion of results and conclusions.

14. SUBJECT TERMS

Turbofans; Ducted fan engines; Fan blades; Fans; Rotating stalls; Flow distortion; Aerodynamics; Blowing; Fluid injection; Extraction

15. NUMBER OF PAGES

62

16. PRICE CODE

17. SECURITY CLASSIFICATION OF REPORT	18. SECURITY CLASSIFICATION OF THIS PAGE	19. SECURITY CLASSIFICATION OF ABSTRACT	20. LIMITATION OF ABSTRACT
Unclassified	Unclassified	Unclassified	